Journal of Medicinal Chemistry

Article

pubs.acs.org/jmc

Toward the Selective Delivery of Chemotherapeutics into Tumor Cells by Targeting Peptide Transporters: Tailored Gold-Based Anticancer Peptidomimetics

Morelle Negom Kouodom,[†] Luca Ronconi,[†] Marta Celegato,[‡] Chiara Nardon,[†,⊥] Luciano Marchiò,[§] Q. Ping Dou,[⊥] Donatella Aldinucci,[‡] Fernando Formaggio,[†] and Dolores Fregona*[,†]

[†]Department of Chemical Sciences, University of Padova, Via F. Marzolo 1, Padova 35131, Italy

[‡]Division of Experimental Oncology 2, Centro di Riferimento Oncologico (CRO-IRCCS), Via F. Gallini 2, Aviano (PN) 33081, Italy

[§]Department of Chemistry, University of Parma, Parco Area delle Scienze 17A, Parma 43100, Italy

[⊥]The Developmental Therapeutics Program, Departments of Oncology, Pharmacology and Pathology, Barbara Ann Karmanos Cancer Institute, School of Medicine, Wayne State University, 540.1 HWCRC, 4100 John R Road, Detroit, Michigan 48201, United States

Supporting Information

ABSTRACT: Complexes [$Au^{III}X_2$(dtc-Sar-AA-O(*t*-Bu))] (AA = Gly, X = Br (**1**)/Cl (**2**); AA = Aib, X = Br (**3**)/Cl (**4**); AA = L-Phe, X = Br (**5**)/Cl (**6**)) were designed on purpose in order to obtain gold(III)-based anticancer peptidomimetics that might specifically target two peptide transporters (namely, PEPT1 and PEPT2) upregulated in several tumor cells. All the compounds were characterized by means of FT-IR and mono- and multidimensional NMR spectroscopy, and the crystal structure of [$Au^{III}Br_2$(dtc-Sar-Aib-O(*t*-Bu))] (**3**) was solved and refined. According to in vitro cytotoxicity studies, the Aib-containing complexes **3** and **4** turned out to be the most effective toward all the human tumor cell lines evaluated (PC3, DU145, 2008, C13, and L540), reporting IC_{50} values much lower than that of cisplatin. Remarkably, they showed no cross-resistance with cisplatin itself and were proved to inhibit tumor cell proliferation by inducing either apoptosis or late apoptosis/necrosis depending on the cell lines. Biological results are here reported and discussed in terms of the structure−activity relationship.

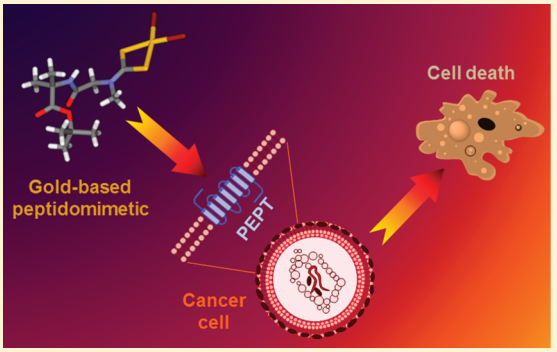

INTRODUCTION

Platinum drugs are well-established as effective anticancer agents, the forerunner being cisplatin.[1] Although their therapeutic effectiveness is severely hindered by some adverse side-effects, such as neuro- and nephrotoxicity and tumor resistance (either intrinsic or acquired during cycles of therapy),[2] the unquestionable clinical success of cisplatin and its second- and third-generation analogues has triggered the development of several alternative metal-based potential anticancer agents.[3,4]

Overall, gold compounds are currently gaining ground as a new class of chemotherapeutics owing to their strong tumor cell growth inhibiting effect, generally achieved by exploiting noncisplatin-like pharmacodynamic and pharmacokinetic properties and mechanisms of action.[5] In particular, gold(III) complexes share with platinum(II) derivatives some key chemical features, such as the preference for square-planar geometry and the typical d^8 electronic configuration, making them attractive for testing as antineoplastic drugs. Furthermore, due to their traditional use in medicine for the treatment of rheumatoid arthritis (chrysotherapy),[6] gold(III) derivatives are natural candidates as potential alternatives to clinically established platinum drugs. In fact, their antiarthritic activity arises from the well-known immunosuppressive and antiinflammatory actions, thus establishing, at least in principle, a connection between the two therapies.[7]

In this context, we have previously reported on some gold(III)−dithiocarbamato derivatives of the type [$Au^{III}X_2$(dtc)] (X = Cl, Br; dtc = various dithiocarbamates) designed in such a way to reproduce very closely the main features of cisplatin. The choice of dithiocarbamato ligands is not accidental; in fact, dithiocarbamates have been successfully used as chemoprotectants to modulate cisplatin nephrotoxicity without decreasing its antitumor activity.[8] These gold(III) compounds were shown to exert outstanding in vitro cytotoxicity, even toward human tumor cell lines intrinsically resistant to cisplatin, and no cross-resistance to the reference platinum drug.[9,10] In this regard, for the first time, we have identified the proteasome as a major in vitro and in vivo

Received: November 2, 2011
Published: February 6, 2012

Chart 1. Dipeptides and the Corresponding Gold(III)−Dithiocarbamato Complexes Studied in this Work

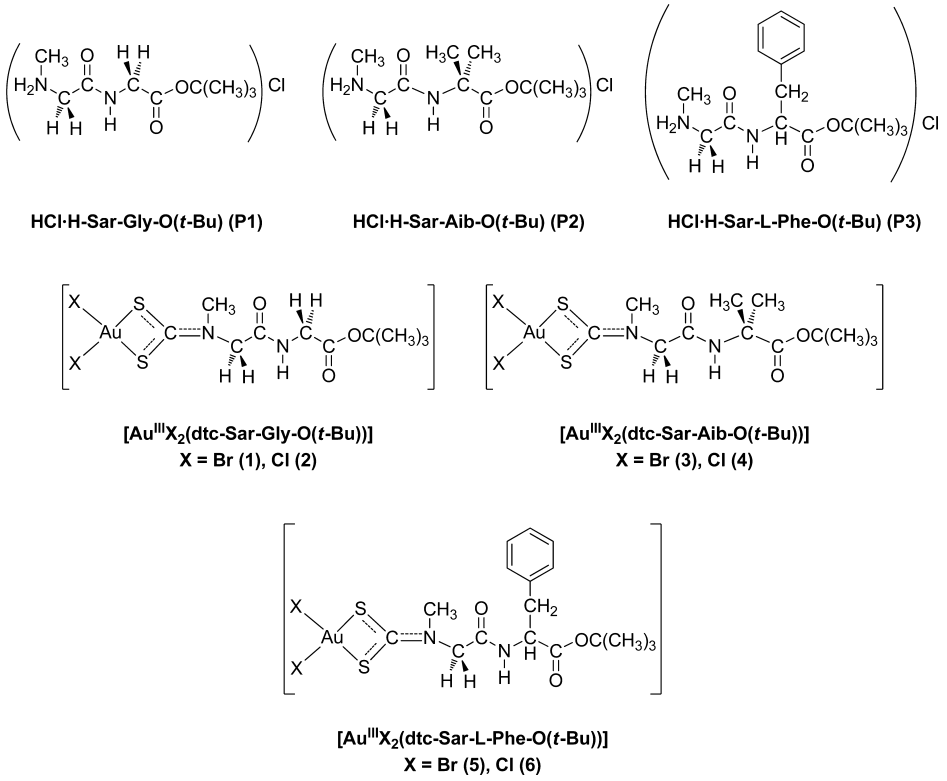

target,[11,12] thus suggesting a different mechanism of action compared to that of platinum drugs. Remarkably, their chemotherapeutic properties have been confirmed in vivo,[11,13] together with negligible acute toxicity and almost lack of nephrotoxic side-effects,[14] thus supporting the rationale of our strategy.

Subsequent to the positive achieved outcomes, we have extended our research toward "second-generation" gold(III)−dithiocarbamato derivatives of dipeptides as improved intracellular drug transfer and delivery systems supported by transport proteins. A major problem of therapeutic effectiveness relies on the crossing of the cell membrane. Cellular uptake of therapeutics is still a challenging task because of the plasma membrane, which constitutes an impermeable barrier for most molecules. In order to overcome this issue, several carrier-mediated delivery strategies have been investigated. Among them, much attention has been recently given to peptide-based delivery systems. Peptide transporters are integral plasma membrane proteins that mediate the cellular uptake of di- and tripeptides and peptide-like drugs (i.e., peptidomimetics). Two peptide transporters, namely PEPT1 and PEPT2, have been identified in mammals. They are present predominantly in epithelial cells of the small intestine, bile duct, mammary glands, lung, choroid plexus, and kidney but are also localized in other tissues (pancreas, liver, gastrointestinal tract) and, intriguingly, seem to be overexpressed in some types of tumors.[15] A unique feature is their capability for sequence-independent transport of most possible di- and tripeptides inside the cells. These transporters are stereoselective toward peptides containing L-enantiomers of amino acids. Apart from degradation products of nutritional proteins, some peptidomimetic (e.g., bestatin, L-dopa), nonpeptidic (e.g., valacyclovir, AZT, 5-aminolevulinic acid) drugs and prodrugs, β-lactam antibiotics (e.g., cefadrine, cefadroxil, cyclacillin, cefixime, ceftibuten), and some angiotensin-converting enzyme (ACE) inhibitors, such as fosinopril, captopril and enalapril, are recognized by either PEPT1 or PEPT2 as substrates because of their resemblance to di- or tripeptides.[16] Therefore, peptide transporters represent excellent targets for the delivery of pharmacologically active compounds because their substrate binding site can accommodate a wide range of molecules with different size, hydrophobicity, and charge.[17]

On account of these considerations, the rationale of our research was to design gold(III) complexes of the type $[Au^{III}X_2(dpdtc)]$ (X = Cl, Br; dpdtc = dipeptidedithiocarbamate) which could both preserve the antitumor properties and reduce toxic and nephrotoxic side-effects of the previously reported gold(III) analogues,[9,10] together with an enhanced bioavailability and tumor selectivity due to the dipeptide-mediated cellular internalization provided by PEPTs. Accordingly, we report here on the synthesis, chemical characterization, and in vitro anticancer activity of the gold(III)−dipeptidedithiocarbamato derivatives $[Au^{III}X_2$(dtc-Sar-AA-O(*t*-Bu))] (X = Cl, Br; AA = Gly, Aib, L-Phe). Biological results are discussed in terms of the structure−activity relationship, focusing on the potential outcome of this novel class of metal-based peptidomimetics.

RESULTS

Chemistry. *Syntheses.* Three *tert*-butyl-esterified dipeptides were prepared as hydrochlorides (HCl·H-Sar-AA-O(*t*-Bu), AA = Gly (**P1**), Aib (**P2**), L-Phe (**P3**)) and used to synthesize the corresponding gold(III)−dithiocarbamato derivatives $[Au^{III}X_2$(dtc-Sar-AA-O(*t*-Bu))] (X = Cl, Br; AA = Gly, Aib, L-Phe (**1**−**6**)) (Chart 1).

Compounds **P1**−**P3**, being short peptides, were prepared by classical solution (not on solid support) strategies,[18−21] in order to obtain large amounts of the final products. With reference to

dx.doi.org/10.1021/jm201480u | J. Med. Chem. 2012, 55, 2212−2226

Scheme 1, the first step was the *tert*-butyl esterification of the Z-protected amino acid (Z-AA-OH) through the acid-catalyzed

Scheme 1. Synthetic Scheme for the Preparation of Dipeptides HCl·H-Sar-AA-O(*t*-Bu) (AA = Gly (P1), Aib (P2), L-Phe (P3))[a]

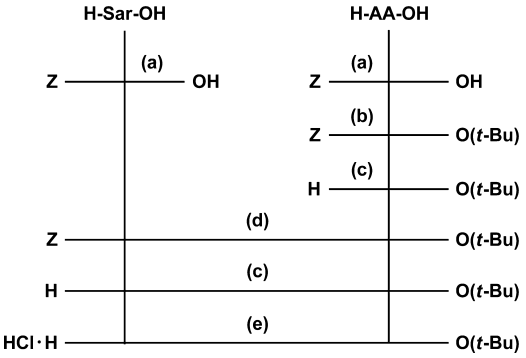

[a](a) ZOSu, TEA, CH_3CN/H_2O, r.t., 4 d; (b) isobutene, H_2SO_4 (cat.), CH_2Cl_2, −60 °C/r.t., 7 d; (c) 10% Pd−C, H_2, MeOH; (d) NMM, isobutyl chloroformiate, THF/$CHCl_3$, −15 °C to r.t., overnight; (e) HCl/Et_2O.

reaction with isobutene, followed by the removal of the Z-protecting group by catalytic hydrogenation. The dipeptides H-Sar-AA-O(*t*-Bu) were then obtained by condensation of Z-Sar-OH with H-AA-O(*t*-Bu) and subsequent catalytic hydrogenation. The resulting purified products were finally isolated as hydrochlorides by slow addition of 1 equiv of dilute HCl in diethyl ether. This procedure avoided the hydrolysis of the *tert*-butyl ester and, consequently, increased yields as well as reduced the occurrence of side products.

The gold(III)−dithiocarbamato complexes **1**−**6** were prepared as previously reported.[22] The main synthetic route to dithiocarbamates is based on the base-catalyzed nucleophilic attack of a primary or secondary amine to carbon disulfide.[23] This process can even take place without using a strong base, but, in this case, the yield is much lower and the reaction slower.[24] All attempts to isolate the dithiocarbamato derivatives of dipeptides **P1**−**P3** without causing their degradation during the separation/purification process were proved unsuccessful, so the gold(III) complexes **1**−**6** were obtained by a template reaction involving two steps. With reference to Scheme 2, during the first step, the dithiocarbamic acid of a dipeptide forms in solution owing to the reaction in water of the starting dipeptide hydrochloride with carbon disulfide and sodium hydroxide in equimolar ratio, the pH consequently turning from 10 to approximately 6 as the reaction proceeds. The solution is subsequently reacted with 0.5 equiv of $K[Au^{III}X_4]$ (X= Br, Cl) in water, leading to the sudden precipitation of the expected gold(III) complex in good yields (70−90%).

Characterization. The starting dipeptides and the corresponding gold(III)−dithiocarbamato derivatives were characterized by means of several techniques in order to assess the structure as well as to investigate their stability in solution.

The proposed stoichiometry of the gold complexes was confirmed by both elemental and thermogravimetric analyses, the latter indicating a good correlation between calculated and found weight loss values to metallic gold (Table S1 in the Supporting Information).

IR spectroscopy was proved useful to identify the synthesized complexes. With reference to Table 1, by comparison with the spectra recorded for the starting dipeptide ester hydrochlorides **P1**−**P3**, the disappearance of the broad band at 2680−2780 cm^{-1} ($\nu_{a/s}(NH_2^+)$)[25] together with the detection of two new absorption bands at around 1560 (ν(N−CSS), somewhat overlapped with amide II) and at ca. 1000 cm^{-1} (ν_a(S−C−S)) in the spectra of the corresponding gold derivatives **1**−**6**, is consistent with the formation of gold(III)−dithiocarbamato complexes in which the NCSS moiety chelates the metal center in a symmetrical bidentate mode.[22] Such coordination is also supported by the presence of two bands in the range 380−420 cm^{-1} associated with the $\nu_{a/s}$(S−Au−S).[26] Finally, the two remaining coordination sites are taken up by *cis*-halides (either Br or Cl), as confirmed by the appearance of two new bands at 315−360/215−255 cm^{-1} related to the $\nu_{a/s}$(X−Au−X) (X = Cl, Br, respectively).[27,28] Remarkably, the other main frequencies originated by the dipeptide chains seem not to be affected by the formation of the dithiocarbamate and the subsequent metal coordination, except for a significant increase of the ν(N−H) together with a shift of the amide II band toward lower wavenumbers.

The NMR characterization was carried out by means of mono- (^{1}H, Table 2) and multidimensional ([^{1}H,^{13}C] HMBC, Table 3) techniques. Compared with the spectra of the starting dipeptide ester hydrochlorides **P1**−**P3**, those recorded for the corresponding gold complexes **1**−**6** show a general shift of all the signals toward higher δ values. The downfield shift increases with the closeness to the NCSS moiety, the larger variation (ca. 1 ppm) involving the methyl and the methylene groups directly bound to the dithiocarbamato nitrogen atom. Only for the amide proton peaks lower chemical shift values (ca. 1 ppm) were recorded. Moreover, the disappearance of the NH_2^+ proton signal, together with the detection of a new ^{13}C signal at about 200 ppm (assigned to the dithiocarbamato carbon atom),[29] is consistent with the formation of the gold(III)−peptide derivatives depicted in Chart 1. Interestingly, in all the

Scheme 2. . Template Reaction Involved in the Preparation of the Complexes $[Au^{III}X_2$(dtc-Sar-AA-O(*t*-Bu))][a]

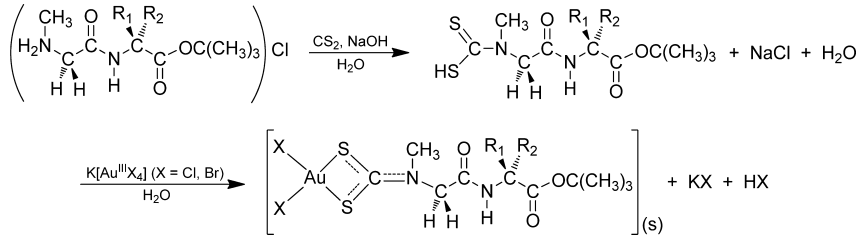

[a](X/AA ⇒ Br/R_1 = R_2 = H: Gly (**1**); Cl/R_1 = R_2 = H: Gly (**2**); Br/R_1 = R_2 = CH_3: Aib (**3**); Cl/R_1 = R_2 = CH_3: Aib (**4**); Br/R_1 = H, R_2 = CH_2Ph: L-Phe (**5**); Cl/R_1 = H, R_2 = CH_2Ph: L-Phe (**6**)).

dx.doi.org/10.1021/jm201480u | J. Med. Chem. 2012, 55, 2212−2226

Table 1. Selected IR Frequencies of the Starting Dipeptides P1−P3 and the Corresponding Gold(III)−Dithiocarbamato Derivatives 1−6

	vibrational mode [cm^{-1}]									
compound	ν NH	$\nu_{a/s}$ NH_2^+	ν C=O	amide I	ν N−CSS	amide II	amide III	$\nu_{a/s}$ SCS	$\nu_{a/s}$ SAuS	$\nu_{a/s}$ XAuX
P1	3307	2777/2709	1732	1669	–	1576	1258	–	–	–
1	3352	–	1736	1673	1568[a]		1252	1006/557	418/387	252/217[b]
2	3349	–	1737	1672	1561[a]		1253	1006/558	418/384	358/322[c]
P2	3292	2744/2683	1736	1689	–	1563	1259	–	–	–
3	3362	–	1734	1690	1560	1531	1259	996/545	411/383	252/223[b]
4	3365	–	1733	1691	1563	1534	1252	996/547	412/383	347/316[c]
P3	3300	2775/2704	1737	1666	–	1543	1254	–	–	–
5	3331		1731	1683	1558[a]		1259	997/562	408/381	252/220[b]
6	3341		1733	1684	1559[a]		1256	999/563	408/383	359/326[c]

[a] ν(N−CSS) and amide II overlapped. [b] X = Br. [c] X = Cl.

Table 2. ^{1}H NMR Spectral Data of the Starting Dipeptides P1−P3 (HCl·H-Sar-AA-O(*t*-Bu), AA = Gly, Aib, L-Phe) and the Corresponding Gold(III)−Dithiocarbamato Derivatives 1−6 ([$Au^{III}X_2$(dtc-Sar-AA-O(*t*-Bu))], X = Cl, Br; AA = Gly, Aib, L-Phe)

	$\delta(^1H)$ [ppm]				
			Sar		
compound	(*t*-Bu)O	AA	CH_3N	CH_2N	NH_2^+
		AA = Gly			
P1[a]	1.41 ($(CH_3)_3C$)	3.82 (CH_2)	2.53	3.72	8.99
		8.91 (*NH*)			
1[b]	1.45 ($(CH_3)_3C$)	3.95/3.97 (CH_2)	3.53/3.57	4.71/4.75	–
		7.93 (*NH*)			
2[b]	1.45 ($(CH_3)_3C$)	3.95/3.97 (CH_2)	3.56/3.57	4.75	–
		7.92 (*NH*)			
		AA = Aib			
P2[a]	1.38 ($(CH_3)_3C$)	1.35 ($(CH_3)_2C$)	2.52	3.64	9.05
		8.84 (*NH*)			
3[b]	1.44 ($(CH_3)_3C$)	1.45/1.46 ($(CH_3)_2C$)	3.51/3.54	4.63/4.66	–
		7.90 (*NH*)			
4[b]	1.44 ($(CH_3)_3C$)	1.45/1.46 ($(CH_3)_2C$)	3.54/3.55	4.66	–
		7.88 (*NH*)			
		AA = L-Phe			
P3[a]	1.33 ($(CH_3)_3C$)	2.89−3.04 (CH_2Ph)	2.44	3.62	8.80
		4.40−4.46 (*CH*)			
		7.25−7.30 (*Ph*)			
		8.92 (*NH*)			
5[b]	1.43 ($(CH_3)_3C$)	2.98−3.20 (CH_2Ph)	3.45/3.49	4.65/4.70	–
		4.67−4.74 (*CH*)			
		7.25−7.33 (*Ph*)			
		7.91 (*NH*)			
6[b]	1.43 ($(CH_3)_3C$)	2.98−3.20 (CH_2Ph)	3.49	4.70	–
		4.67−4.74 (*CH*)			
		7.25−7.33 (*Ph*)			
		7.92 (*NH*)			

[a] DMSO-d_6. [b] Acetone-d_6.

complexes, the sarcosine residue ($C(O)CH_2N(CH_3)CSS$) gives rise to two sets of signals (both in ^{1}H and ^{13}C spectra), suggesting the coexistence of two different forms, in agreement with data previously reported for analogous compounds.[22,30] Intriguingly, one interconverts into the other over time, and the rate of such a conversion strongly depends on the solvent, that is, it occurs in acetone but not in DMSO (see Discussion).

X-ray Crystal Structure. The X-ray crystal structure of [$Au^{III}Br_2$(dtc-Sar-Aib-O(*t*-Bu))] (**3**) is shown in Figure 1. The corresponding crystallographic data as well as a list of selected bond lengths and angles are reported in Table S2 and Table S3, respectively, in the Supporting Information.

The gold(III) complex adopts a distorted square-planar geometry achieved through the bidentate dithiocarbamato ligand and the two *cis*-bromides. The four donor atoms and the metal center lie on a plane, and the distortion from the ideal geometry is a consequence of the small bite angle of the dithiocarbamato moiety (ca. 75°). The Au−S distances (2.316(2) and 2.313(3) Å) are approximately 0.1 Å shorter than those of Au−Br (2.439(2) and 2.440(1) Å). The dithiocarbamato nitrogen atom is functionalized with two

dx.doi.org/10.1021/jm201480u | J. Med. Chem. 2012, 55, 2212−2226

Table 3. ^{13}C NMR Spectral Data of the Starting Dipeptides P1−P3 (HCl·H-Sar-AA-O(*t*-Bu), AA = Gly, Aib, L-Phe) and the Corresponding Gold(III)−Dithiocarbamato Derivatives 1−6 ([$Au^{III}X_2$(dtc-Sar-AA-O(*t*-Bu))], X = Cl, Br; AA = Gly, Aib, L-Phe)

	δ(^{13}C) [ppm]					
			Sar			
compound	(*t*-Bu)O	AA	CH_3N	CH_2N	CO	CSS
		AA = Gly				
P1[a]	27.5 ($(CH_3)_3C$)	41.1 (CH_2)	32.4	48.6	165.6	–
	80.8 ($(CH_3)_3C$)	168.4 (CO)				
1[b]	28.7 ($(CH_3)_3C$)	43.1 (CH_2)	40.1/41.1	55.1/59.0	165.1/165.4	197.7/200.5
	82.6 ($(CH_3)_3C$)	169.9 (CO)				
2[b]	28.7 ($(CH_3)_3C$)	43.2 (CH_2)	40.7/41.1	55.6	165.1	195.5/200.6
	82.7 ($(CH_3)_3C$)	169.8 (CO)				
		AA = Aib				
P2[a]	27.3 ($(CH_3)_3C$)	25.4 ($(CH_3)_2C$)	32.4	48.6	164.2	–
	79.9 ($(CH_3)_3C$)	55.8 ($(CH_3)_2C$)				
		172.2 (CO)				
3[b]	28.6 ($(CH_3)_3C$)	25.6 ($(CH_3)_2C$)	40.2/41.2	55.3/56.2	164.0	196.6/200.3
	81.9 ($(CH_3)_3C$)	58.4 ($(CH_3)_2C$)				
		173.7 (CO)				
4[b]	28.5 ($(CH_3)_3C$)	25.5 ($(CH_3)_2C$)	40.6/41.0	55.7	163.8	195.1/200.2
	81.9 ($(CH_3)_3C$)	58.2 ($(CH_3)_2C$)				
		173.6 (CO)				
		AA = L-Phe				
P3[a]	27.5 ($(CH_3)_3C$)	36.9 (CH_2Ph)	32.8	49.2	165.8	–
	81.1 ($(CH_3)_3C$)	54.3 (CH)				
		126−137 (*Ph*)				
		170.2 (CO)				
5[b]	28.1 ($(CH_3)_3C$)	38.5 (CH_2Ph)	39.7/40.7	54.7/55.6	164.1/164.3	196.1/199.3
	82.6 ($(CH_3)_3C$)	55.2 (CH)				
		128−138 (*Ph*)				
		170.8 (CO)				
6[b]	27.9 ($(CH_3)_3C$)	38.3 (CH_2Ph)	40.5	55.3	164.0/164.1	194.5/199.6
	82.3 ($(CH_3)_3C$)	55.0 (CH)				
		127−138 (*Ph*)				
		170.9 (CO)				

[a]DMSO-d_6. [b]Acetone-d_6.

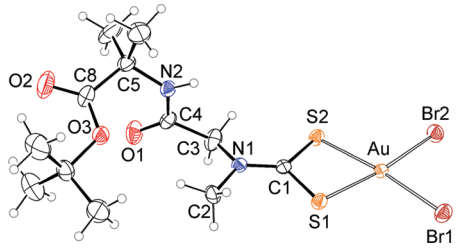

Figure 1. X-ray crystal structure with atom numbering scheme for [$Au^{III}Br_2$(dtc-Sar-Aib-O(*t*-Bu))] (**3**), with thermal ellipsoids drawn at 30% probability.

distinct residues, that is, the *N*-methyl group (C(2)) and the dipeptide chain (comprising an amide and a *tert*-butyl ester function). The conformation adopted by the latter is such that the planar amide and the ester groups form an angle of approximately 74°, and the *tert*-butyl group is spatially close to the sarcosine *N*-methyl moiety. The projection of the crystal packing along the *c* crystallographic axis (Figure 2A) reveals the presence of two distinct zones defined by two types of weak interactions, the first characterized by the antiparallel superimposition of the coordination planes and the second associated with the hydrophobic interaction between the peripheral *tert*-butyl substituents. In addition, couples of

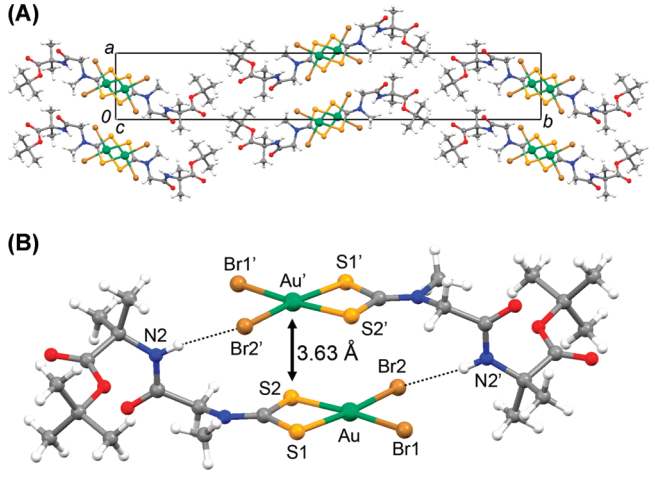

Figure 2. (A) Crystal packing of [$Au^{III}Br_2$(dtc-Sar-Aib-O(*t*-Bu))] (**3**) projected along the *c* crystallographic axis. (B) Depiction of the hydrogen bonds formed between two symmetry-related molecules (N(2)−Br(2)′ = 3.791(8) Å).

symmetry-related molecules form two weak hydrogen bonds between the amide group (N(2)) and one gold(III)-bound bromide belonging to an adjacent molecule (Br(2)′).

dx.doi.org/10.1021/jm201480u | *J. Med. Chem.* 2012, 55, 2212−2226

Table 4. Growth Inhibition of Human Prostate Cancer (PC3 and DU145), Ovarian Adenocarcinoma Cisplatin-Sensitive (2008) and -Resistant (C13), and Hodgkin's Lymphoma (L540) Cells by Gold(III)−Dipeptidedithiocarbamato Derivatives 1−6 and Comparison with That by Reference Drugs Cisplatin and [$Au^{III}Br_2$(dtc-Sar-OEt)] (over 72 h)

	IC_{50} [μM]				
compound	PC3	DU145	2008	C13	L540
cisplatin	3.3 ± 0.3	4.5 ± 0.1	19.4 ± 1.2	117.2 ± 9.1	2.5 ± 0.1
1	1.3 ± 0.1	4.5 ± 0.9	18.0 ± 1.6	11.5 ± 1.2	2.1 ± 0.2
2	1.6 ± 0.1	2.5 ± 0.3	13.2 ± 1.1	15.9 ± 1.3	3.4 ± 0.2
3	0.8 ± 0.1	1.4 ± 0.1	4.5 ± 0.2	3.7 ± 0.3	1.5 ± 0.2
4	1.1 ± 0.1	2.2 ± 0.1	4.7 ± 0.2	5.1 ± 0.4	1.7 ± 0.3
5	16.8 ± 1.7	13.2 ± 1.2	41.2 ± 4.0	17.2 ± 1.8	16.4 ± 1.5
6	16.5 ± 1.6	15.3 ± 1.5	43.4 ± 3.8	21.5 ± 1.5	7.3 ± 0.5
[$Au^{III}Br_2$(dtc-Sar-OEt)]	0.4 ± 0.1[a]	1.1 ± 0.2[a]	4.5 ± 0.9[b]	2.8 ± 0.4[b]	–

[a]Reference 13. [b]Reference 22.

Biological Activity. *In Vitro Cytotoxicity.* As a preliminary screening, the in vitro cytotoxic activity of complexes **1**−**6** was investigated toward the human androgen receptor-negative prostate cancer PC3 and DU145 cells, ovarian adenocarcinoma 2008 cells and the parent cisplatin-resistant C13 cell line, and Hodgkin's lymphoma L540 cells (Table 4). The inhibition of cell proliferation was evaluated over 72 h by means of the trypan blue dye exclusion test for the floating L540 cells, and the BrdU ELISA assay (allowing cell proliferation to be assessed by quantifying DNA synthesis during cells activation and proliferation) for adherent prostate and ovarian cancer cell lines. Results are expressed in terms of IC_{50} values and compared to the results from reference drug cisplatin as well as from the gold(III)−dithiocarbamato analogue [$Au^{III}Br_2$(dtc-Sar-OEt)] previously reported,[13,22] tested under the same experimental conditions.

Exposure of L540 cells to increasing concentrations of complexes **1**−**4** resulted in a remarkable inhibition of cell growth, with IC_{50} values (1.5−3.4 μM) comparable to that recorded for cisplatin (2.5 μM). The same gold(III) derivatives exhibited more potent cytotoxicity on both prostate cancer cell lines, with IC_{50} values up to 4- and 3-fold lower than cisplatin in PC3 and DU145 cells, respectively. The ovarian adenocarcinoma 2008 cells appeared to be less sensitive to the treatment than prostate cancer and lymphoma cells. Nonetheless, compounds **1**−**4** induced a massive dose-dependent inhibition of cell proliferation, in particular complexes **3** and **4**, for which IC_{50} values of 4.5 and 4.7 μM, respectively, were observed (ca. four times as active as cisplatin). Conversely, the gold(III) derivatives **5** and **6** did not exhibit significant cytotoxicity.

When tested on the cisplatin-resistant C13 cell line, the gold(III) complexes reported here (including **5** and **6**) were proved much more active than the reference drug, the best performers being complexes **3** and **4**, for which IC_{50} values are up to 31-fold lower than that for cisplatin.

Induction of Apoptosis. The capability to induce apoptosis was then tested by incubating the various cancer cell lines with a single cytotoxic dose (10 μM for PC3/DU145/L540 cells, 30 μM for 2008/C13 cells) of compounds **1**−**6** or cisplatin for 24 h. With reference to Figure 3, treatment of both PC3 and DU145 prostate cancer cells with complexes **3** and **4** resulted in a substantial phosphatidylserine exposure (as evident from the much higher amount of FITC-Annexin-V stained cells compared to FITC-Annexin-V/PI stained ones), supporting apoptosis as the primary mechanism involved in cell growth inhibition. Conversely, cisplatin and the other gold(III) derivatives showed modest or even no activity under the same experimental conditions (except for a weak effect on PC3 cells by complexes **1** and **2**).

Analogously, compounds **3** and **4** were proved the most effective toward human ovarian adenocarcinoma cells. Remarkably, the induction of apoptosis was shown to be the major mechanism of cell death on the cisplatin-resistant C13 cell line, whereas on the corresponding sensitive parent cell line (2008), a higher percentage of cells underwent late apoptosis/necrosis (as confirmed by the massive amount of FITC-Annexin-V/PI stained cells). Again, the other gold(III) complexes, as well as cisplatin, induced negligible effect on this type of tumor cells.

Finally, the L540 cell line was the most sensitive to the treatment. In particular, compounds **1**−**4** were proved to inhibit cell proliferation mainly by inducing late apoptosis/necrosis, whereas the effect of complexes **5** and **6** and cisplatin was negligible.

DISCUSSION

A major success story during the past 40 years of metallopharmaceuticals relates to cisplatin and its second generation derivatives carboplatin and oxaliplatin.[31] Since the 1970s, platinum-based chemotherapeutics have had a major impact as anticancer drugs and are still widely used today, particularly for genitourinary cancers.[1] However, their use is restricted by severe toxicity as well as by intrinsic or acquired resistance.[32] Accordingly, a massive number of other metal compounds has been extensively investigated over the years, aimed at overcoming these drawbacks. In this regard, some gold(III) complexes have shown interesting biological properties and are believed to operate through mechanisms of action different from those of platinum drugs in clinical use.[33]

Recently, the emphasis in cancer drug development has been shifting from cytotoxic nonspecific chemotherapies to molecularly targeted rationally designed drugs promising greater effectiveness and less side-effects.[34] The "magic bullet" concept (as first proposed by Ehrlich)[35] may be summarized in one word: targeting. Targeting and delivery are two aspects of drug design that have been receiving much attention in recent years because of the potential for improving efficacy and reducing unwanted side-effects.[36] Tumor cells express many biomarkers and receptors that can be specifically targeted by cytotoxic agents. Conjugated drugs incorporating a tumor targeting group and a cytotoxic "smart bomb" are emerging as promising therapies for cancer treatment. In particular, this approach has been successfully used for peptide-mediated delivery of metal complexes into cells.[37]

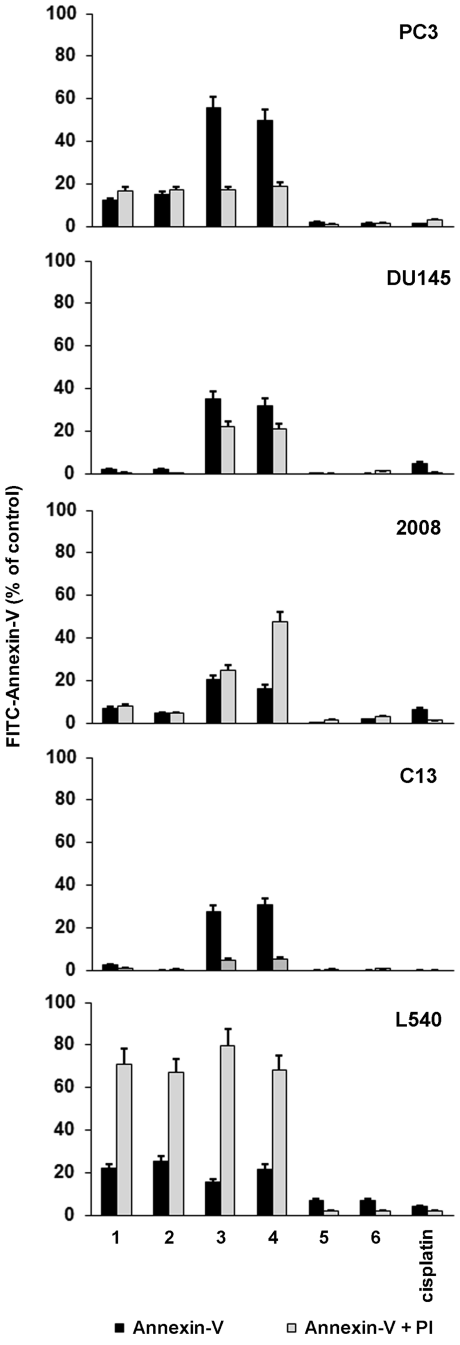

Figure 3. FACS analysis of cells after 24 h incubation at 37 °C with either complexes **1**–**6** or cisplatin (10 μM for PC3/DU145/L540 cells, 30 μM for 2008/C13 cells) and double stained with FITC-Annexin-V and PI.

In this context, the proton-coupled peptide transporters PEPT1 and PEPT2 are currently under intense investigation. Owing to their capability to promote the cellular uptake of physiologically occurring di- and tripeptides, they can internalize into the cells suitable peptidomimetic substrates with therapeutic properties or precursors of pharmacologically active agents.[15−17] Notwithstanding the exceptionally broad substrate specificity, these membrane proteins are unable to transport free amino acids or larger peptides, and some specific constraints must be fulfilled by substrates to be recognized. Most of all possible natural di- and tripeptides can be accepted, excluding those containing N-terminal proline residues[38] and the tripeptide Trp-Trp-Trp.[39] Peptides consisting solely of L-amino acids are preferred over D-analogues, and those consisting of D-stereoisomers only are not transported.[38,40]

When xenobiotics are taken into account as possible substrates (i.e., peptidomimetics), the following essential and affinity-determining features have to be identified for their recognition:[15]

(1) A peptide bond is not required but, when present, it must be in trans conformation.
(2) The N- and the C-terminus have to be separated by 500−635 pm.
(3) A free N-terminal amino group is preferred for recognition by PEPT2 (but not required by PEPT1), whereas the C-terminal carboxylic group is not essential and can be replaced by a hydrophobic function.
(4) The more hydrophobic the side chain, the higher the affinity to PEPT2; conversely, charged side chains provide higher affinity for PEPT1.

Although sharing the same physiological functions and having similar substrate specificity, PEPT1 and PEPT2 essentially differ in the overall transport characteristics, the former representing a low affinity but high transport capacity system whereas the latter is a high affinity but low capacity transporter.[17] Moreover, peptidomimetics can act as either substrates to be internalized or "competitors" recognized but not transported inside the cell, just inhibiting further uptake of other di- and tripeptides.[16] For instance, PEPT1 and PEPT2 were shown to have high and medium affinity (in terms of affinity constant K_i), respectively, toward the antiviral prodrug valganciclovir, which acts as a substrate to be transported in the first case but as an inhibitor in the latter.[41]

So far, peptide symporters PEPT1 and PEPT2 have been localized in some mammalian tissues/organs, such as small intestine, kidney, pancreas, bile duct, liver, mammary glands, and lung.[16] On the other hand, cancer cells require larger amounts of peptide-bound amino acids for growth and metabolism, and consequently peptide transporters might be upregulated.[42] In this regard, it was recently reported that PEPTs are ubiquitously overexpressed in various types of tumor cells but not in the corresponding healthy tissues,[43,44] thus representing a suitable specific target for the delivery of pharmacologically active peptidomimetics.

On account of these assumptions, we have been developing some gold(III)−dithiocarbamato peptidomimetics that can combine both the anticancer activity and the favorable toxicological profile of the gold(III) analogues previously studied,[45] with an improved tumor selectivity by targeting PEPT1 and/or PEPT2 via the dipeptide chain. The basic idea relies on the potential recognition of the whole metal complex that, once recognized and transported by PEPTs and delivered inside the tumor cell, could exert its anticancer activity without affecting healthy tissues.

Design and Structure of the Complexes. According to the objectives outlined above, we designed three dipeptides of the type HCl·H-Sar-AA-O(*t*-Bu) (AA = Gly, Aib, L-Phe; **P1**−**P3**) and successfully synthesized the corresponding gold(III)−dipeptidedithiocarbamato derivatives [$Au^{III}X_2$(dtc-Sar-AA-O(*t*-Bu))] (X = Cl, Br; **1**−**6**) depicted in Chart 1.

The choice of the dipeptides was not accidental. We first decided to maintain the sarcosinedithiocarbamato moiety to resemble our "first generation" gold(III) analogues.[22] Moreover, the sarcosine-containing dipeptide Gly-Sar is often used as

reference substrate for peptide transport studies because of its good affinity toward both PEPT1 and PEPT2.[46] The terminal amino acids were chosen to evaluate how flexibility (Gly), rigidity (Aib), chirality and hydrophobicity (L-Phe) could modulate the biological activity of the various complexes. Finally, esterification of the C-terminus was proved necessary because it was previously shown that analogues containing a free carboxylic function are not active.[29] Additionally, although conferring less water solubility, the bulky *tert*-butyl group is unlikely to undergo easy hydrolysis (occurring only in strongly acidic conditions), thus providing stability to the final compounds and, consequently, avoiding intramolecular cyclization of the dipeptide chain.

IR spectroscopy provided insights into both the structural characterization and the coordination mode of complexes **1**−**6** (Table 1). Peptide bonds C(O)N(H) give rise to several vibrational modes that may be regarded as diagnostic for some structural features. In particular, those referred to as amide I and amide II show relatively strong infrared absorptions and are very sensitive to the formation of hydrogen bonds.[47] The amide I mode is mainly assigned to the in-plane peptide carbonyl stretching and is generally observed between 1620 and 1660 cm^{-1} for H-bonded carbonyls or at higher frequencies (1660−1710 cm^{-1}) for "free" C═O groups.[48] Conversely, the major contribution to amide II band is given by the in-plane N−H bending, and its detection in the range 1500−1520 cm^{-1} is consistent with "free" N−H groups, whereas the presence of hydrogen bonds induces a shift toward higher wavenumbers (1540−1570 cm^{-1}).[49] As concerns the starting dipeptides **P1**−**P3**, the position of the amide I bands is consistent with non-hydrogen-bonded peptide carbonyl groups, and this feature is maintained in the corresponding gold(III)−dithiocarbamato derivatives. On the contrary, in all cases the amide N−H groups seem to be involved in the formation of hydrogen bonds, although their strength decreases when moving from free dipeptides to the gold(III) counterparts (as confirmed by the shift of the amide II band of the complexes toward lower frequencies). This is also supported by the behavior of the broad band at ca. 3300 cm^{-1} assigned to the stretching of trans peptide N−H groups, which shifts toward slightly higher wavenumbers in the complexes (compared to the associated free dipeptides), accounting for less strong hydrogen bonds.[50] Bands related to the other groups located in the dipeptide backbones farther from the metal center seem to be negligibly affected by the formation of the metal complexes.

IR spectra also provide useful information about the metal coordination. Complexes **1**−**6** exhibit a characteristic strong absorption at around 1560 cm^{-1} (primarily associated with the "thioureide" band due to the ν(N−CSS)), consistent with chelating dithiocarbamato ligands coordinated to a gold(III) metal center.[22]

The detection of a single band at ca. 1000 cm^{-1} in all the gold(III) complexes (commonly attributed to the ν_a(S−C−S)) is a clear indication for the symmetrical bidentate coordination of the dithiocarbamato moieties to the metal center, as based on the Bonati−Ugo criterion.[51]

New bands, absent in the IR spectra of the free dipeptides **P1**−**P3**, were observed in the range 380−420 cm^{-1} and assigned to gold(III)−sulfur stretching vibrations, in agreement with data previously reported.[22] Finally, other informative bands were recorded at lower wavenumbers (215−360 cm^{-1}), attributed to the metal−halide stretching modes for terminal *cis*-chlorides/bromides.[22,26]

This structural hypothesis was confirmed by the X-ray crystal structure of complex **3** (Figure 1) whose square-planar geometry around the gold(III) center with two *cis*-halides is fully consistent with IR data, as well as the occurrence of hydrogen bonds involving the peptide amide group (Figure 2B).

NMR Spectroscopy and Solution Chemistry. The synthesized dipeptides **P1**−**P3** and the complexes **1**−**6** were characterized by ^{1}H (Table 2) and ^{13}C (Table 3) NMR spectroscopy. A general downfield shift of the proton signals is observed for the dipeptide backbone upon formation of the corresponding gold(III)−dithiocarbamato derivatives, the greater variation involving sarcosine *N*-methyl and *N*-methylene groups. On moving away from the NCSS moiety, the chemical shift change diminishes until being negligible for the *tert*-butyl ester group. This trend, in agreement with data previously reported,[22] is also maintained for ^{13}C signals. In this regard, the most significant carbon-13 peaks are those recorded at ca. 200 ppm and attributed to the dithiocarbamic carbon atoms. The δ(N^{13}CSS) values are normally detected in the range 190−215 ppm, and it is generally assumed that they are strongly dependent on both the type of the dithiocarbamate−metal bonding and the oxidation state of the metal center.[52] For high oxidation state transition metal derivatives such as gold(III), ^{13}C peaks are found at 193−201 ppm.[53] There is a strong empirical correlation between δ(N^{13}CSS) values and the carbon−nitrogen stretching vibrations in the IR spectra. Higher ν(N−CSS) frequencies are associated with higher degrees of carbon−nitrogen double bond character, which correlate well with lower δ(N^{13}CSS) values owing to lower total π-bond orders.[52] These considerations are consistent with experimental results reported here for all the compounds **1**−**6**.

The solution chemistry of the gold(III)−dipeptidedithiocarbamato complexes was investigated in-depth in order to evaluate their stability. As examples, the ^{1}H NMR spectra of complex **1** in acetone-d_6 (Figure 4) and in DMSO-d_6 (Figure 5)

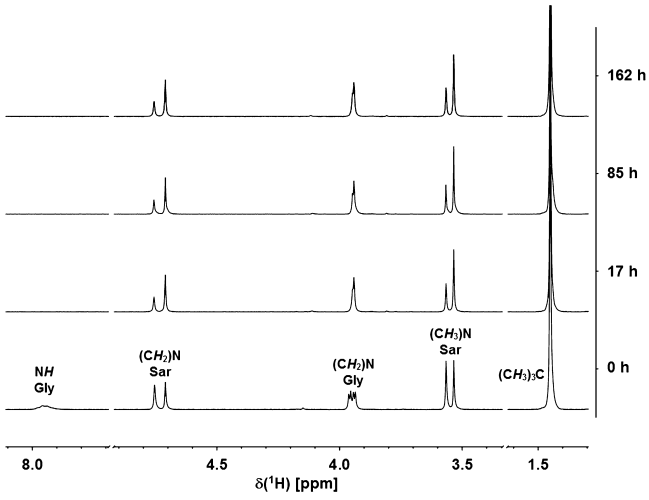

Figure 4. ^{1}H NMR spectra of complex **1** in acetone-d_6 over time.

over time are discussed. First of all, after 17 h, the ^{1}H signal of the amide proton is not detectable anymore in acetone-d_6, leading to the subsequent simplification of the multiplicity of the vicinal glycine α-methylene protons. Such an unexpected experimental evidence is likely to be due to the possible hydrogen/deuterium exchange with solvent. Peptide amides are

dx.doi.org/10.1021/jm201480u | J. Med. Chem. 2012, 55, 2212−2226

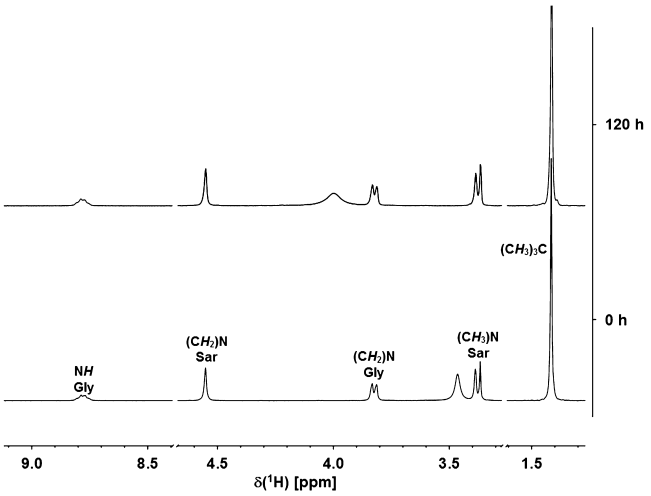

Figure 5. ^{1}H NMR spectra of complex **1** in DMSO-d_6 over time.

well-known to easily undergo hydrogen exchange reactions with protic deuterated solvents (e.g., D_2O and methanol-d_4),[54] whereas, to the best of our knowledge, it is not reported for aprotic deuterated solvents. On the other hand, it is apparent that such an exchange reaction occurs for complex **1** in acetone-d_6 (Figure 4) and that it is clearly solvent-dependent because it does not take place in DMSO-d_6 (Figure 5). As far as we are aware, a similar behavior has been reported only once for a zinc(II) complex coordinated to an amide-like-containing ligand.[55]

It is also worth noting that two sets of signals are detected for *N*-methyl and *N*-methylene functions belonging to the sarcosine residue. With reference to Figure 4, soon after dissolution of complex **1** in acetone-d_6, two ^{1}H signals at 3.53/3.57 and 4.71/4.75 ppm are observed, for sarcosine NCH_3 and NCH_2 groups respectively, at approximately 1:1 ratio. Intriguingly, the downfield peaks interconvert into their highfield counterparts over time, progressively decreasing in intensity and reaching a sort of equilibrium within 85 h (the final ratio being ca. 1:3). The coexistence of two different forms of compound **1** is also confirmed by the presence of two signals for the NCSS carbon atom in the [^{1}H,^{13}C] HMBC spectrum (Figure 6), each giving rise to long-range couplings with one set

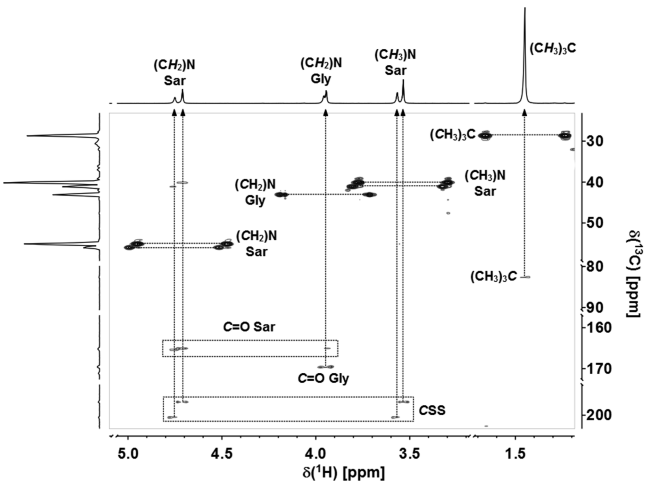

Figure 6. [^{1}H,^{13}C] HMBC spectrum of complex **1** in acetone-d_6.

of *N*-methyl and *N*-methylene sarcosine groups. Two forms have been observed also in DMSO-d_6 but, remarkably, there is no interconversion of one into the other over time (Figure 5), confirming the crucial role of the solvent in the solution behavior. The major species in solution is likely to be the expected gold(III)−dithiocarbamato derivative **1** depicted in Chart 1, whereas the identification of the second species is still uncertain, although this behavior has been previously reported and discussed for some analogues.[22] The same results were obtained for all the other complexes **2**−**6**, no matter what the dipeptide chain or the halide type (data not shown).

Effects of Gold Complexes on Cancer Cell Proliferation. Complexes **1**−**6** were tested for in vitro cytotoxicity toward human prostate cancer (PC3 and DU145), Hodgkin's lymphoma (L540), and ovarian adenocarcinoma cisplatin-sensitive (2008) and -resistant (C13) cell lines over 72 h. For comparison purposes, cisplatin was also evaluated as a reference.

So far, the peptide transporters PEPT1 and PEPT2 have not been localized in either the normal genitourinary apparatus or healthy lymphocytes.[16] Therefore, according to our designing strategy (see above), we first evaluated their expression in the selected tumor cells by incubation with rabbit polyclonal IgG PEPT1- or PEPT2-specific antibodies, followed by FITC-conjugated antirabbit IgG. Remarkably, both peptide transporters were shown to be expressed to a good extent in all five tumor cell lines (as assessed by FACS analysis, Figure 7), thus

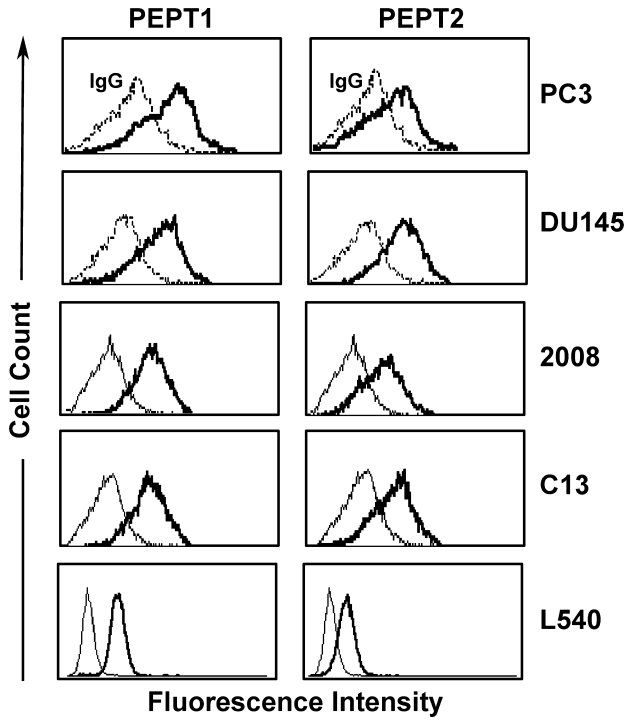

Figure 7. FACS analysis of PEPT1 and PET2 surface expression in human prostate cancer (PC3 and DU145), ovarian adenocarcinoma cisplatin-sensitive (2008) and -resistant (C13), and Hodgkin's lymphoma (L540) cells after incubation with rabbit polyclonal IgG PEPT1- or PEPT2-specific antibodies (1:100 dilution), followed by FITC-conjugated AffiniPure F(ab′)2 fragment donkey antirabbit IgG (H+L) (1:50 dilution). Dotted lines indicate background fluorescence of cells, as determined by isotype-matched immunoglobulins or autofluorescence. *X*- and *Y*-axes indicate the logarithms of the relative intensity of fluorescence and relative cell number, respectively.

dx.doi.org/10.1021/jm201480u | J. Med. Chem. 2012, 55, 2212−2226

making them suitable for preliminary screening of the anticancer activity of our gold(III)−dipeptidedithiocarbamato derivatives.

With reference to Table 4, compounds **5** and **6** were less active, showing IC_{50} values higher than cisplatin. Apparently, an aromatic or too hydrophobic moiety next to sarcosine appears to be detrimental to the activity of the complexes.

The remaining gold(III) complexes were generally more effective than the reference drug, the derivative **3** turning out to be the best performer on all the investigated tumor cell lines. In particular, it was proved about 30-fold more active than cisplatin in inhibiting cell proliferation of cisplatin-resistant ovarian adenocarcinoma C13 cells, ruling out the occurrence of cross-resistance phenomena.

The capability of the most active complexes **3** and **4** to inhibit cell proliferation was also evaluated after shorter exposure times (i.e., 24 h) on prostate cancer PC3 and DU145 cells (data not shown). Remarkably, for both compounds, IC_{50} values turned out to be fully comparable to those here reported after 72 h, thus confirming that they exert their cytotoxic activity within the first 24 h or even less. Conversely, as expected, cisplatin was much less active after 24 h exposure, with IC_{50} values 5- and 3-fold higher toward PC3 and DU145 cells, respectively (compared to data obtained after 72 h).

The evidence that Aib-containing complexes **3** and **4** showed a higher cytotoxic effect is not surprising. The α-amino-isobutyric acid is a natural noncoded amino acid and is abundant in a class of peptide antibiotics (namely, antibiotic peptaibols) exhibiting antiviral and anticancer activity.[56,57] It was recently suggested that Aib plays a crucial role in the biological activity of peptaibols because it forces the peptide backbone to fold into helical arrangements, providing a relevant capability to cross and/or perturb cell membranes.[58] Therefore, the presence of an Aib residue in compound **3** might increase its bioavailability and, consequently, the biological activity. Remarkably, its corresponding IC_{50} values are comparable to those reported for the "first generation" analogue [$Au^{III}Br_2$(dtc-Sar-OEt)] toward the same tumor cell lines (Table 4), thus confirming that the favorable anticancer properties are preserved notwithstanding the modification of the organic chain.

Induction of Apoptosis. Although the mechanism of action of the object gold(III) derivatives is still under investigation, we tested their capability to inhibit human tumor cell proliferation by inducing apoptosis using the Annexin-V/PI double staining assay over 24 h (Figure 3). One of the earliest features of apoptosis is the translocation of the plasma membrane phospholipid phosphatidylserine (PS) from the inner to the outer leaflet of the membrane itself, thereby exposing PS to the external environment. The phospholipid binding protein Annexin-V specifically binds to PS exposed on the cell surface and, once detected by flow cytometry, it allows the identification of early stage apoptotic cells. Remarkably, the relative integrity of the membrane of cells undergoing early apoptosis prevents internalization of PI. On the other hand, because of extensive membrane damage, necrotic cells are quickly stained by both Annexin-V and PI, thus allowing the differentiation between early apoptotic and necrotic cells. Anyway, a major drawback of this assay is that as apoptosis progresses and the plasma membrane becomes compromised (i.e., late apoptotic cells) PI is also internalized. Therefore, for longer exposure times there is no clear-cut parameter to distinguish by flow cytometry between cells undergoing either necrosis or late apoptosis.

On account of these remarks, focusing on the most active complexes **3** and **4**, apoptosis was shown to be the major mechanism of cell death for prostate cancer PC3 and DU145 cells and for ovarian adenocarcinoma cisplatin-resistant C13 cells. Conversely, for the parent cisplatin-sensitive 2008 cells as well as for the Hodgkin's lymphoma L540 cell line, the majority of dead cells appeared to undergo late apoptosis/necrosis over 24 h. As previously mentioned, owing to the fact that these complexes might exert their cytotoxic activity within the first 24 h or even less (see above), we cannot rule out the hypothesis that cells first undergo early apoptosis but, as the process goes on, after 24 h it is not possible to distinguish between late apoptotic and necrotic cells. The other gold(III) complexes, as well as cisplatin, were proved less or negligibly effective in inducing apoptosis except for a weak effect on PC3 and L540 cells by complexes **1** and **2**.

All together, these preliminary results confirm that the most active gold(III)−dipeptidedithiocarbamato derivatives exert their cancer cell growth-inhibitory activity by exploiting different mechanisms of action compared to the reference drug cisplatin and are able to overcome the onset of acquired resistance.

CONCLUSIONS

Killing cancer cells is easy, but achieving this goal without affecting healthy cells and without impairing the normal physiological body functions is not trivial. Cancer cells are well-known to overexpress some specific biomarkers and receptors needed for carcinogenesis and tumor growth; therefore, target chemotherapies aim to block cancer cell proliferation by interfering with such specific upregulated molecules. In this regard, membrane peptide transporters PEPT1 and PEPT2 were proved to be upregulated in several tumor types and, owing to their capability to promote the cellular uptake of potentially all physiologically occurring di- and tripeptides, they can also internalize peptide-like chemotherapeutics resembling the main structural features of small peptides (i.e., peptidomimetics). Thus, they represent an excellent target for the site-specific delivery of pharmacologically active substrates acting as "Trojan horses".

In order to develop an innovative metal-based target chemotherapy, in the present work we explore the rational design of some gold(III)−dipeptidedithiocarbamato peptidomimetics of the type [$Au^{III}X_2$(dtc-Sar-AA-O(*t*-Bu))] (X = Cl, Br; AA = Gly, Aib, L-Phe; **1**−**6**, Chart 1) designed on purpose to combine the well-known anticancer properties of the gold(III) metal center and the intrinsic chemoprotective function of coordinated dithiocarbamates, with an enhanced bioavailability and tumor selectivity through the dipeptide-mediated cellular internalization by exploiting membrane transporters PEPT1 and PEPT2.

Complexes **1**−**6** were fully characterized both in solid state and in solution, and the X-ray crystal structure of derivative **3** was obtained and discussed. Preliminary in vitro cytotoxicity tests were carried out on human prostate (PC3 and DU145), ovarian adenocarcinoma (2008), and Hodgkin's lymphoma (L540) cells, some of them showing promising anticancer activity with IC_{50} values up to 5-fold lower than that of the reference drug cisplatin toward all the investigated cell lines. When cisplatin-resistant ovarian adenocarcinoma C13 cells were tested, activity levels comparable to those observed on the

parent sensitive 2008 cells were detected for all the gold(III) derivatives, thus ruling out the occurrence of cross resistance with cisplatin (Table 4). Overall, the Aib-containing derivatives **3** and **4** turned out to be the best performers and, remarkably, apoptosis was the major mechanism involved in the growth inhibition of PC3, DU145 and cisplatin-resistant C13 cells. Conversely, they exerted their cytotoxic effect on L540 and cisplatin-sensitive 2008 cells mainly by inducing late apoptosis/necrosis over 24 h (Figure 3). All together, these results are likely to account for a different mechanism of action compared to that of clinically established platinum drugs.

As a further extension of our previous research on gold(III)−dithiocarbamato anticancer agents,[59] this work aims to develop "second generation" gold(III) compounds that are able to maintain both the outstanding antitumor activity and the favorable nephrotoxicity and acute toxicity levels of their previous analogues, together with an improved selectivity toward tumor cells. The real breakthrough is not simply the use of gold compounds to treat cancer but the rational design of gold-based drugs which may be very effective, nontoxic, and potentially selective toward cancer cells, their enormous potential impact relying on the possible site-specific delivery in localized cancers, thus strongly improving the cellular uptake and minimizing unwanted side-effects. As far as we are aware of, this appears to be the first time that metal-based peptidomimetic anticancer agents are designed specifically to target peptide transporters. Eventually, this idea appears to be an original and innovative strategy in order to develop novel and more selective chemotherapeutic agents that could provide a valuable alternative to the platinum-based anticancer drugs in clinical use.

Complexes **1** and **3** are currently under investigation for their in vivo anticancer activity as well as for the elucidation of their mechanism of action. Should they really resemble the behavior of their previous analogues, we are expecting the proteasome to be a major biological target, and preliminary outcomes seem to confirm this hypothesis.

These results represent a solid starting point for the recognition of this class of gold(III) peptidomimetics as suitable candidates for further pharmacological testing and, remarkably, allowed us to file an international patent for their use in cancer chemotherapy (just extended in several countries worldwide).[60]

EXPERIMENTAL SECTION

Materials. Sarcosine, L-phenylalanine, *N*-methylmorpholine, palladium catalyst (10% on activated charcoal), TEA (Fluka), isobutyl chloroformiate (Lancaster), Z-Gly-OH, Z-Aib-OH, DMSO, DMSO-d_6, acetone-d_6, carbon disulfide, propidium iodide, trypan blue (Aldrich), cisplatin (Pharmacia and Upjohn), isobutene (Siad), ZOSu (Iris Biotech), potassium tetrachloro- and tetrabromoaurate(III) dihydrate (Alfa Aesar), RPMI medium, penicillin, streptomycin, L-glutamine (Cambrex Bio Science), and fetal bovine serum (Gibco) were of reagent grade or comparable purity and were used as supplied. All other reagents and solvents were used as purchased without any further purification.

Instrumentation. *Melting Points.* Melting points were determined using a Stuart SMP10 apparatus and were not corrected.

Chromatography. Thin layer chromatography was performed on silica gel Merck Kieselgel 60F_{254} precoated glass plates. Retention factors (R_f) were measured using either chloroform/ethanol 9:1 (R_{f1}) or 1-butanol/acetic acid/water 3:1:1 (R_{f2}) or toluene/ethanol 7:1 (R_{f3}) as eluents. Spots were visualized by direct UV irradiation at 254 nm or developed by exposure to either iodine vapors or NaClO/ninhydrin chromatic reaction as appropriate. Flash column chromatography was performed on MercK Kiesegel 60 silica gel (40−63 μm, 230−400 mesh) as stationary phase.

Polarimetric Measurements. Optical rotations were measured at 546 nm in spectrophotometric grade methanol at 20 °C using a Perkin-Elmer 241 polarimeter equipped with a Haake D thermostat and a cell with an optical pathway of 10 cm.

Elemental Analysis. CHNS elemental analyses were carried out on either a Fisons EA-1108 CHNS-O or a Perkin-Elmer 2400 CHN microanalyzer.

IR Spectroscopy. FT-IR spectra were recorded in nujol on a Nicolet Nexus 870 spectrophotometer (1000 scans, resolution 2 cm^{-1}) for the range 50−600 cm^{-1} and in solid KBr on either a Nicolet 55XC or a Perkin-Elmer 580B spectrophotometer (32 scans, resolution 2 cm^{-1}) for the range 400−4000 cm^{-1}. Data processing was carried out using OMNIC version 5.1 (Nicolet Instrument Corporation).

NMR Spectroscopy. All NMR spectra were acquired in the appropriate deuterated solvent at 298 K on a Bruker Avance DRX300 spectrometer using a BBI [^{1}H,X] probe-head equipped with *z*-field gradients. Data processing was carried out using MestReNova version 6.2 (Mestrelab Research S.L.). Typical acquisition parameters for 1D ^{1}H NMR spectra (^{1}H: 300.13 MHz): 16 transients, spectral width 7.5 kHz, using 32 k data points and a delay time of 5.0 s. Spectra were processed using exponential weighting with a resolution of 0.5 Hz and a line-broadening threshold of 0.1 Hz. Typical acquisition parameters for 2D [^{1}H,^{13}C] HMBC NMR spectra (^{1}H: 300.13/^{13}C: 75.48 MHz): 512 transients of 32 scans/block, spectral width 7.5/18.8 kHz, 2k/2k data points and a delay time of 2.0 s. Sequences were optimized for $^1J(^{13}C,^1H)$ = 145 Hz/$^nJ(^{13}C,^1H)$ = 5 Hz with no ^{1}H decoupling. Spectra were processed by using sine-square weighting with a resolution of 1.0/3.0 Hz and a line-broadening threshold of 0.3/1.0 Hz. ^{1}H and ^{13}C chemical shifts were referenced to TMS at 0.00 ppm via internal referencing to the residual peak of the deuterated solvent employed.[61]

Thermogravimetric Analysis. Thermogravimetric (TG) and differential scanning calorimetry (DSC) curves were recorded with a TA Instruments thermobalance equipped with a DSC 2929 calorimeter. Measurements were carried out in the range 25−1000 °C in alumina crucibles under air (flux rate 30 cm^3 min^{-1}) at a heating rate of 5 °C min^{-1}, using alumina as a reference.

X-ray Crystallography. Single crystal diffraction data were collected at 293(2) K with a Bruker Smart APEXII diffractometer using Mo Kα radiation. The unit cell parameters were obtained using 60 ω-frames of 0.5° width and scanned from three different zones of reciprocal lattice. Intensity data were integrated from several series of exposure frames (0.3° width) covering the sphere of reciprocal space.[62] Absorption corrections were applied using SADABS,[63] which gave minimum and maximum transmission factors of 0.573 and 1.000, respectively. The structure was solved by direct methods (SIR2004)[64] and refined on F^2 with full-matrix least-squares (SHELXL-97),[65] using WinGX software package.[66] Non-hydrogen atoms were refined anisotropically, and hydrogen atoms were added at calculated positions. Graphical material was prepared with ORTEP-3 for Windows.[67]

A summary of data collection and structure refinement for complex **3** is reported in the Supporting Information (Table S2). X-ray crystallographic data have been deposited at the Cambridge Crystallographic Data Center and allocated the deposition number CCDC 848402, and the corresponding CIF file can be obtained free of charge from http://www.ccdc.cam.ac.uk.

Syntheses. The purity of all the synthesized compounds was ≥95% as determined by elemental and thermogravimetric analyses.

Synthesis of Dipeptides and Related Intermediates. Z-Sar-OH, Z-L-Phe-OH, and Z-AA-O(*t*-Bu) (AA = Gly, L-Phe, Aib) were prepared according to literature methods (see Supporting Information for details).[18,19]

General Synthetic Route to tert-Butyl-Esterified Dipeptide Hydrochlorides. A THF solution (15−20 mL) of Z-Sar-OH is treated with NMM (1 equiv), cooled to −15 °C and then treated with IBCF (1 equiv) under stirring.[20] After 10 min, a cold suspension of H-AA-O(*t*-Bu) (AA = Gly, L-Phe, Aib, 1 eq; obtained by previous catalytic

hydrogenation in CH_2Cl_2 of the corresponding Z-protected derivative)[21] in $CHCl_3$ (10−35 mL) is added and the pH adjusted to ca. 8 with NMM. After being stirred overnight at room temperature, the reaction mixture is concentrated under reduced pressure, the residue taken up with AcOEt, washed with 10% $KHSO_4$, H_2O, 5% $NaHCO_3$, H_2O, and dried over Na_2SO_4. The organic layer is then concentrated to dryness and the product purified by flash chromatography using AcOEt/petroleum ether 1:1 as eluent, to obtain the corresponding Z-Sar-AA-O(*t*-Bu) (yield = 70−90%).

Each Z-Sar-AA-O(*t*-Bu) intermediate is then Z-deprotected by catalytic hydrogenation in MeOH, and an ether solution of the corresponding H-Sar-AA-O(*t*-Bu) is dropwise treated with 1 equiv of a dilute ether solution of HCl under stirring. Eventually, the solvent is evaporated to dryness, the residue taken up with fresh ether and filtered, and the solvent removed, yielding the corresponding dipeptide hydrochloride HCl·H-Sar-AA-O(*t*-Bu) (AA = Gly, L-Phe, Aib).

HCl·H-Sar-Gly-O(*t*-Bu) (P1). White powder. Yield: 78%. Mp: 129−130 °C. R_{f1}($CHCl_3$/EtOH 9:1): 0.05; R_{f2}(BuOH/AcOH/H_2O 3:1:1): 0.50; R_{f3}(PhMe/EtOH 7:1): 0.05. Anal. Calcd for $C_9H_{19}ClN_2O_3$ (MW = 238.71 g mol^{-1}): C, 45.28; H, 8.02; N, 11.74%; found: C, 45.27; H, 8.18; N, 11.52%. FT-IR (KBr, $\overline{\nu}_{max}$/cm^{-1}): 3307 (ν, N−H); 2777,2709 ($\nu_{a,s}$, NH_2^+); 1732 (ν, C=O_{ester}); 1669 (amide I); 1576 (amide II); 1258 (amide III); 1242 (ν, C−O(*t*-Bu)); 1167 (ν, O−(*t*-Bu)). ^{1}H NMR (DMSO-d_6, 300.13 MHz, TMS, δ/ppm): 1.41 (s, 9H, $(CH_3)_3C$); 2.53 (s, 3H, CH_3N Sar); 3.72 (s, 2H, CH_2N Sar); 3.82 (d, ^3J = 5.8 Hz, 2H, CH_2 Gly); 8.91 (t, ^3J = 5.8 Hz, 1H, N*H* Gly); 8.99 (s br, 2H, NH_2^+ Sar). ^{13}C NMR (DMSO-d_6, 75.48 MHz, TMS, δ/ppm): 27.5 ($(CH_3)_3C$); 32.4 (CH_3N Sar); 41.1 (CH_2 Gly); 48.6 (CH_2N Sar); 80.8 ($(CH_3)_3C$); 165.6 (*C*=O Sar); 168.4 (*C*=O Gly).

HCl·H-Sar-Aib-O(*t*-Bu) (P2). White powder. Yield: 84%. Mp: 156−157 °C. R_{f1}($CHCl_3$/EtOH 9:1): 0.10; R_{f2}(BuOH/AcOH/H_2O 3:1:1): 0.60; R_{f3}(PhMe/EtOH 7:1): 0.05. Anal. Calcd for $C_{11}H_{23}ClN_2O_3$ (MW = 266.78 g mol^{-1}): C, 49.53; H, 8.69; N, 10.50%; found: C, 49.53; H, 8.47; N, 10.37%. FT-IR (KBr, $\overline{\nu}_{max}$/cm^{-1}): 3292 (ν, N−H); 2744,2683 ($\nu_{a,s}$, NH_2^+); 1736 (ν, C=O_{ester}); 1689 (amide I); 1563 (amide II); 1259 (amide III); 1247 (ν, C−O(*t*-Bu)); 1152 (ν, O−(*t*-Bu)). ^{1}H NMR (DMSO-d_6, 300.13 MHz, TMS, δ/ppm): 1.35 (s, 6H, $(CH_3)_2C$ Aib); 1.38 (s, 9H, $(CH_3)_3C$); 2.52 (s, 3H, CH_3N Sar); 3.64 (s, 2H, CH_2N Sar); 8.84 (s, 1H, N*H* Aib); 9.05 (s br, 2H, NH_2^+ Sar). ^{13}C NMR (DMSO-d_6, 75.48 MHz, TMS, δ/ppm): 25.4 ($(CH_3)_2C$ Aib); 27.3 ($(CH_3)_3C$); 32.4 (CH_3N Sar); 48.6 (CH_2N Sar); 55.8 ($(CH_3)_2C$ Aib); 79.9 ($(CH_3)_3C$); 164.2 (*C*=O Sar); 172.2 (*C*=O Aib).

HCl·H-Sar-L-Phe-O(*t*-Bu) (P3). White powder. Yield: 90%. Mp: 80−81 °C. R_{f1}($CHCl_3$/EtOH 9:1): 0.20; R_{f2}(BuOH/AcOH/H_2O 3:1:1): 0.65; R_{f3}(PhMe/EtOH 7:1): 0.10. $[\alpha]_{546}^{20}$ = +7.8° (*c* 0.5, MeOH). Anal. Calcd for $C_{16}H_{25}ClN_2O_3$ (MW = 328.83 g mol^{-1}): C, 58.44; H, 7.66; N, 8.52%; found: C, 58.61; H, 7.78; N, 8.55%. FT-IR (KBr, $\overline{\nu}_{max}$/cm^{-1}): 3300 (ν, N−H); 2775,2704 ($\nu_{a,s}$, NH_2^+); 1737 (ν, C=O_{ester}); 1666 (amide I); 1543 (amide II); 1254 (amide III); 1240 (ν, C−O(*t*-Bu)); 1163 (ν, O−(*t*-Bu)). ^{1}H NMR (DMSO-d_6, 300.13 MHz, TMS, δ/ppm): 1.33 (s, 9H, $(CH_3)_3C$); 2.44 (s, 3H, CH_3N Sar); 2.89−3.04 (m, 2H, CH_2Ph L-Phe); 3.62 (s, 2H, CH_2N Sar); 4.40−4.46 (m, 1H, *CH* L-Phe); 7.25−7.30 (m, 5H, ***Ph*** L-Phe); 8.80 (s br, 2H, NH_2^+ Sar); 8.92 (d, ^3J = 7.1 Hz, 1H, N*H* L-Phe). ^{13}C NMR (DMSO-d_6, 75.48 MHz, TMS, δ/ppm): 27.5 ($(CH_3)_3C$); 32.8 (CH_3N Sar); 36.9 (CH_2Ph L-Phe); 49.2 (CH_2N Sar); 54.3 (*CH* L-Phe); 81.1 ($(CH_3)_3C$); 126.6 (*p*-CH L-Phe); 128.3 (*m*-CH L-Phe); 129.3 (*o*-CH L-Phe); 137.0 (CH_2-*C* L-Phe); 165.8 (*C*=O Sar); 170.2 (*C*=O L-Phe).

General Synthetic Route to Gold(III)−Dipeptidedithiocarbamato Complexes. An aqueous solution of HCl·H-Sar-AA-O(*t*-Bu) (AA = AA = Gly, L-Phe, Aib) is dropwise treated under stirring with CS_2 (1 equiv) and, subsequently, with NaOH (1 equiv). After 2−3 h, pH turns from 10 to ca. 6 according to the reaction pathway depicted in Scheme 2, and the solution is slowly added under stirring to an aqueous solution of K[Au^{III}X$_4$] (0.5 equiv; X = Cl, Br), leading to the sudden precipitation of a solid. The residue is then filtered off, washed with cold water, purified by recrystallization from acetone/water, and dried under reduced pressure with P_2O_5, yielding the corresponding gold derivative [Au^{III}X$_2$(dtc-Sar-AA-O(*t*-Bu))] (X = Cl, Br; AA = Gly, Aib, L-Phe).

[Au^{III}Br$_2$(dtc-Sar-Gly-O(*t*-Bu))] (1, dibromido[1-(1,1-dimethylethyl) *N*-dithiocarboxy-κ*S*,κ*S*′)-*N*-methylglycylglycinato]gold(III)). Dark orange powder. Yield: 77%. Mp: decomposes at 153 °C. Anal. Calcd for $C_{10}H_{17}AuBr_2N_2O_3S_2$ (MW = 634.16 g mol^{-1}): C, 18.94; H, 2.70; N, 4.42; S, 10.11%; found: C, 19.20; H, 2.78; N, 4.42; S, 10.25%. TG (air): calcd weight loss to Au(0) −68.9%; found −68.6%. FT-IR (KBr, $\overline{\nu}_{max}$/cm^{-1}): 3352 (ν, N−H); 1736 (ν, C=O_{ester}); 1673 (amide I); 1568 (ν, N−CSS + amide II); 1252 (amide III); 1228 (ν, C−O(*t*-Bu)); 1161 (ν, O−(*t*-Bu)); 1006 (ν_a, S−C−S). FT-IR (nujol, $\overline{\nu}_{max}$/cm^{-1}): 557 (ν_s, S−C−S); 418,387 ($\nu_{a,s}$, S−Au−S); 252,217 ($\nu_{a,s}$, Br−Au−Br). ^{1}H NMR (acetone-d_6, 300.13 MHz, TMS, δ/ppm): 1.45 (s, 9H, $(CH_3)_3C$); 3.53/3.57 (s, 3H, CH_3N Sar); 3.95/3.97 (d, ^3J = 5.6 Hz, 2H, CH_2 Gly); 4.71/4.75 (s, 2H, CH_2N Sar); 7.93 (t br, ^3J = 5.5 Hz, 1H, N*H* Gly). ^{13}C NMR (acetone-d_6, 75.48 MHz, TMS, δ/ppm): 28.7 ($(CH_3)_3C$); 40.1/41.1 (CH_3N Sar); 43.1 (CH_2 Gly); 55.1/59.0 (CH_2N Sar); 82.6 ($(CH_3)_3C$); 165.1/165.4 (*C*=O Sar); 169.9 (*C*=O Gly); 197.7/200.5 (*C*SS).

[Au^{III}Cl$_2$(dtc-Sar-Gly-O(*t*-Bu))] (2, dichlorido[1-(1,1-dimethylethyl) *N*-dithiocarboxy-κ*S*,κ*S*′)-*N*-methylglycylglycinato]gold(III)). Yellow ochre powder. Yield: 77%. Mp: decomposes at 155 °C. Anal. Calcd for $C_{10}H_{17}AuCl_2N_2O_3S_2$ (MW = 545.26 g mol^{-1}): C, 22.03; H, 3.14; N, 5.14; S, 11.76%; found: C, 22.00; H, 3.23; N, 5.08; S, 11.96%. TG (air): calcd weight loss to Au(0) −63.9%; found −63.7%. FT-IR (KBr, $\overline{\nu}_{max}$/cm^{-1}): 3349 (ν, N−H); 1737 (ν, C=O_{ester}); 1672 (amide I); 1561 (ν, N−CSS + amide II); 1253 (amide III); 1229 (ν, C−O(*t*-Bu)); 1162 (ν, O−(*t*-Bu)); 1006 (ν_a, S−C−S). FT-IR (nujol, $\overline{\nu}_{max}$/cm^{-1}): 558 (ν_s, S−C−S); 418,384 ($\nu_{a,s}$, S−Au−S); 358,322 ($\nu_{a,s}$, Cl−Au−Cl). ^{1}H NMR (acetone-d_6, 300.13 MHz, TMS, δ/ppm): 1.45 (s, 9H, $(CH_3)_3C$); 3.56/3.57 (s, 3H, CH_3N Sar); 3.95/3.97 (d, ^3J = 5.9 Hz, 2H, CH_2 Gly); 4.75 (s br, 2H, CH_2N Sar); 7.92 (s br, 1H, N*H* Gly). ^{13}C NMR (acetone-d_6, 75.48 MHz, TMS, δ/ppm): 28.7 ($(CH_3)_3C$); 40.7/41.1 (CH_3N Sar); 43.2 (CH_2 Gly); 55.6 (CH_2N Sar); 82.7 ($(CH_3)_3C$); 165.1 (*C*=O Sar); 169.8 (*C*=O Gly); 195.5/200.6 (*C*SS).

[Au^{III}Br$_2$(dtc-Sar-Aib-O(*t*-Bu))] (3, dibromido[1-(1,1-dimethylethyl) *N*-dithiocarboxy-κ*S*,κ*S*′)-*N*-methylglycyl-2-methylalaninato]gold(III)). Dark orange powder. Yield: 76%. Mp: decomposes at 167 °C. Anal. Calcd for $C_{12}H_{21}AuBr_2N_2O_3S_2$ (MW = 662.21 g mol^{-1}): C, 21.76; H, 3.20; N, 4.23; S, 9.68%; found: C, 21.73; H, 3.33; N, 4.34; S, 10.37%. TG (air): calcd weight loss to Au(0) −70.3%; found −70.2%. FT-IR (KBr, $\overline{\nu}_{max}$/cm^{-1}): 3362 (ν, N−H); 1734 (ν, C=O_{ester}); 1690 (amide I); 1560 (ν, N−CSS); 1531 (amide II); 1252 (amide III); 1214 (ν, C−O(*t*-Bu)); 1144 (ν, O−(*t*-Bu)); 996 (ν_a, S−C−S). FT-IR (nujol, $\overline{\nu}_{max}$/cm^{-1}): 545 (ν_s, S−C−S); 411,383 ($\nu_{a,s}$, S−Au−S); 252,223 ($\nu_{a,s}$, Br−Au−Br). ^{1}H NMR (acetone-d_6, 300.13 MHz, TMS, δ/ppm): 1.44 (s, 9H, $(CH_3)_3C$); 1.45/1.46 (s, 6H, $(CH_3)_2C$ Aib); 3.51/3.54 (s, 3H, CH_3N Sar); 4.63/4.66 (s, 2H, CH_2N Sar); 7.90 (s, 1H, N*H* Aib). ^{13}C NMR (acetone-d_6, 75.48 MHz, TMS, δ/ppm): 25.6 ($(CH_3)_2C$ Aib); 28.6 ($(CH_3)_3C$); 40.2/41.2 (CH_3N Sar); 55.3/56.2 (CH_2N Sar); 58.4 ($(CH_3)_2C$ Aib); 81.9 ($(CH_3)_3C$); 164.0 (*C*=O Sar); 173.7 (*C*=O Aib); 196.6/200.3 (*C*SS).

[Au^{III}Cl$_2$(dtc-Sar-Aib-O(*t*-Bu))] (4, dichlorido[1-(1,1-dimethylethyl) *N*-dithiocarboxy-κ*S*,κ*S*′)-*N*-methylglycyl-2-methylalaninato]gold(III)). Yellow ochre powder. Yield: 81%. Mp: decomposes at 167 °C. Anal. Calcd for $C_{12}H_{21}AuCl_2N_2O_3S_2$ (MW = 573.31 g mol^{-1}): C, 25.14; H, 3.69; N, 4.89; S, 11.19%; found: C, 25.10; H, 3.84; N, 4.84; S, 11.37%. TG (air): calcd weight loss to Au(0) −65.6%; found −65.4%. FT-IR (KBr, $\overline{\nu}_{max}$/cm^{-1}): 3365 (ν, N−H); 1733 (ν, C=O_{ester}); 1691 (amide I); 1563 (ν, N−CSS); 1534 (amide II); 1252 (amide III); 1214 (ν, C−O(*t*-Bu)); 1146 (ν, O−(*t*-Bu)); 996 (ν_a, S−C−S). FT-IR (nujol, $\overline{\nu}_{max}$/cm^{-1}): 547 (ν_s, S−C−S); 412,383 ($\nu_{a,s}$, S−Au−S); 347,316 ($\nu_{a,s}$, Cl−Au−Cl). ^{1}H NMR (acetone-d_6, 300.13 MHz, TMS, δ/ppm): 1.44 (s, 9H, $(CH_3)_3C$); 1.45/1.46 (s, 6H, $(CH_3)_2C$ Aib); 3.54/3.55 (s, 3H, CH_3N Sar); 4.66 (s, 2H, CH_2N Sar); 7.88 (s, 1H, N*H* Aib). ^{13}C NMR (acetone-d_6, 75.48 MHz, TMS, δ/ppm): 25.5 ($(CH_3)_2C$ Aib); 28.5 ($(CH_3)_3C$); 40.6/41.0 (CH_3N Sar); 55.7 (CH_2N Sar); 58.2 ($(CH_3)_2C$ Aib); 81.9

($(CH_3)_3C$); 163.8 (C=O Sar); 173.6 (*C*=O Aib); 195.1/200.2 (CSS).

[$Au^{III}Br_2$(dtc-Sar-L-Phe-O(*t*-Bu))] (5, dibromido[1-(1,1-dimethylethyl) *N*-dithiocarboxy-κ*S*,κ*S*′)-*N*-methylglycyl-L-phenylalaninato]gold(III)). Dark orange powder. Yield: 72%. Mp: decomposes at 124 °C. Anal. Calcd for $C_{17}H_{23}AuBr_2N_2O_3S_2$ (MW = 721.92 g mol^{-1}): C, 28.19; H, 3.20; N, 3.87; S, 8.85%; found: C, 28.14; H, 3.11; N, 3.87; S, 8.73%. TG (air): calcd weight loss to Au(0) −72.7%; found −72.9%. FT-IR (KBr, $\overline{\upsilon}_{max}/cm^{-1}$): 3331 (ν, N−H); 1731 (ν, C=O_{ester}); 1683 (amide I); 1558 (ν, N−CSS + amide II); 1259 (amide III); 1214 (ν, C−O(*t*-Bu)); 1155 (ν, O−(*t*-Bu)); 997 (ν_a, S−C−S). FT-IR (nujol, $\overline{\upsilon}_{max}/cm^{-1}$): 562 ($\nu_s$, S−C−S); 408,381 ($\nu_{a,s}$, S−Au−S); 252,220 ($\nu_{a,s}$, Br−Au−Br). ^{1}H NMR (acetone-d_6, 300.13 MHz, TMS, δ/ppm): 1.43 (s, 9H, $(CH_3)_3C$); 2.98−3.20 (m, 2H, CH_2Ph L-Phe); 3.45/3.49 (s, 3H, CH_3N Sar); 4.65/4.70 (s, 2H, CH_2N Sar); 4.67−4.74 (m, 1H, C*H* L-Phe); 7.25−7.33 (m, 5H, *Ph* L-Phe); 7.91 (d, ^3J = 7.9 Hz, 1H, N*H* L-Phe). ^{13}C NMR (acetone-d_6, 75.48 MHz, TMS, δ/ppm): 28.1 ($(CH_3)_3C$); 38.5 (CH_2Ph L-Phe); 39.7/40.7 (CH_3N Sar); 54.7/55.6 (CH_2N Sar); 55.2 (CH L-Phe); 82.6 ($(CH_3)_3C$); 127.9 (*p*-CH L-Phe); 129.4 (*m*-CH L-Phe); 130.4 (*o*-CH L-Phe); 137.7 (CH_2-*C* L-Phe); 164.1/164.3 (C=O Sar); 170.8 (C=O L-Phe); 196.1/199.3 (CSS).

[$Au^{III}Cl_2$(dtc-Sar-L-Phe-O(*t*-Bu))] (6, dichlorido[1-(1,1-dimethylethyl) *N*-dithiocarboxy-κ*S*,κ*S*′)-*N*-methylglycyl-L-phenylalaninato]gold(III)). Light brown powder. Yield: 82%. Mp: decomposes at 138 °C. Anal. Calcd for $C_{17}H_{23}AuCl_2N_2O_3S_2$ (MW = 635.38 g mol^{-1}): C, 32.14; H, 3.65; N, 4.41; S, 10.09%; found: C, 32.21; H, 3.65; N, 4.40; S, 9.95%. TG (air): calcd weight loss to Au(0) −69.0%; found −69.1%. FT-IR (KBr, $\overline{\upsilon}_{max}/cm^{-1}$): 3341 (ν, N−H); 1733 (ν, C=O_{ester}); 1684 (amide I); 1559 (ν, N−CSS + amide II); 1256 (amide III); 1213 (ν, C−O(*t*-Bu)); 1155 (ν, O−(*t*-Bu)); 999 (ν_a, S−C−S). FT-IR (nujol, $\overline{\upsilon}_{max}/cm^{-1}$): 563 ($\nu_s$, S−C−S); 408,383 ($\nu_{a,s}$, S−Au−S); 359,326 ($\nu_{a,s}$, Cl−Au−Cl). ^{1}H NMR (acetone-d_6, 300.13 MHz, TMS, δ/ppm): 1.43 (s, 9H, $(CH_3)_3C$); 2.98−3.20 (m, 2H, CH_2Ph L-Phe); 3.49 (s, 3H, CH_3N Sar); 4.70 (s, 2H, CH_2N Sar); 4.67−4.74 (m, 1H, C*H* L-Phe); 7.25−7.33 (m, 5H, *Ph* L-Phe); 7.92 (d, ^3J = 7.8 Hz, 1H, N*H* L-Phe). ^{13}C NMR (acetone-d_6, 75.48 MHz, TMS, δ/ppm): 27.9 ($(CH_3)_3C$); 38.3 (CH_2Ph L-Phe); 40.5 (CH_3N Sar); 55.0 (CH L-Phe); 55.3 (CH_2N Sar); 82.3 ($(CH_3)_3C$); 127.5 (*p*-CH L-Phe); 129.2 (*m*-CH L-Phe); 130.4 (*o*-CH L-Phe); 137.7 (CH_2-C L-Phe); 164.0/164.1 (C=O Sar); 170.9 (C=O L-Phe); 194.5/199.6 (CSS).

Biological Activity. *Cell Lines and Culture Conditions.* Hodgkin's lymphoma (L540) and human androgen-resistant prostate cancer (PC3 and DU145) cell lines were obtained from the German Collection of Microorganisms and Cell Cultures (Braunschweig, Germany). Human ovarian adenocarcinoma (2008) cell line was kindly provided by Prof. G. Marverti (University of Modena, Italy). The parent cisplatin-resistant subclone (C13) was obtained by weekly treatment of 2008 cells with 1 μM cisplatin.[68] All cells were cultured at 37 °C in 5% CO_2 and moisture-enriched atmosphere in RPMI medium supplemented with 10% heat-inactivated FBS, 0.1% (w/v) L-glutamine and antibiotics (0.2 mg mL^{-1} penicillin and streptomycin).

Evaluation of Peptide Transporter Expression. PEPT1 and PEPT2 expression in the human tumor cell lines investigated here (PC3, DU145, L540, 2008, C13) were incubated with rabbit polyclonal IgG PEPT1-specific (H-235, 200 μg mL^{-1}) or PEPT2-specific (H-245, 200 μg mL^{-1}) antibodies (Santa Cruz Biotechnology, Santa Cruz, CA) at a dilution of 1:100, followed by FITC-conjugated AffiniPure F(ab′)2 fragment donkey antirabbit IgG (H+L) (1.5 mg mL^{-1}, Jackson ImmunoResearch Europe, UK) at a dilution of 1:50, according to the manufacturer's protocol.[69] Viable antibody-labeled cells were identified according to their forward and right-angle scattering, electronically gated and analyzed on a FACScalibur flow cytometer (Becton-Dickinson, Franklin Lakes, NJ), using CellQuest software (Becton-Dickinson).

Samples Preparation. Before use, gold(III) complexes **1**−**6** and cisplatin were dissolved in DMSO, aliquoted, and stored at −80 °C. Just before the experiments, calculated amounts of drug solutions were added to RPMI medium and filter sterilized, to a final DMSO amount lower than 0.5% (v/v). All the tested gold(III) compounds were proved by ^{1}H NMR to be stable in DMSO over 48 h (Figure S1 in the Supporting Information).

Cell Proliferation Assay. Amounts of 2.5 × 10^3 PC3 or DU145 cells, and 4.0 × 10^3 2008 or C13 cells, were seeded in 96-well flat-bottomed microplates in RPMI medium (100 μL) and incubated at 37 °C in 5% CO_2 atmosphere for 24 h (to allow cell adhesion) before drug testing. The medium was then removed and replaced with fresh medium containing the compounds to be tested (previously dissolved in DMSO, see above) at increasing concentrations (0.3, 0.6, 1.25, 2.5, 5, 10, 20, 40, 80 μM) at 37 °C for 72 h. Each treatment was performed in triplicate. Cell proliferation for cell lines was assayed using the BrdU Cell Proliferation ELISA kit (Roche Diagnostics, Germany), according to the manufacturer's protocol.[70] Alternatively, 2.0 × 10^5 L540 cells mL^{-1} were seeded in 24-well plates and treated as previously described. After the treatment, the viable cells were evaluated by the trypan blue dye exclusion test.[71] Negative exponential dose−response curves were obtained by linear regression and IC_{50} values (i.e., the half maximal inhibitory concentration representing the concentration of a substance required for 50% inhibition in vitro) calculated.

Evaluation of Apoptosis. Amounts of 2.5 × 10^5 PC3 or DU145 or 2008 or C13 cells, and 2.0 × 10^5 L540 cells mL^{-1} were incubated in six-well Petri dishes with RPMI medium supplemented with 10% FBS as is (control) or containing 10 μM (30 μM for both cisplatin-sensitive and -resistant human ovarian adenocarcinoma cells) of either gold complexes **1**−**6** or cisplatin at 37 °C for 24 h. Cells were then harvested and resuspended in 50 μL of binding buffer (10 mM HEPES/NaOH pH 7.4, 140 mM NaCl, 2.5 mM $CaCl_2$), incubated with 5 μL of FITC-conjugated Annexin-V (Pharmigen, USA) in the dark for 15 min, and assayed after the addition of 0.3 mL of binding buffer and 10 μL of propidium iodide (10 μg mL^{-1} in binding buffer) to each sample. Apoptosis induction was assessed by flow cytometry detection of Annexin-V-labeled cells according to their forward and right-angle scattering, electronically gated and analyzed on a FACScalibur flow cytometer (Becton-Dickinson), using CellQuest software (Becton-Dickinson), as described elsewhere.[72]

Statistical Analyses. All values are given as means ± SD of three measurements from three independent experiments. Statistical comparisons were drawn using Student's *t* test. Differences were considered significant where $p < 0.05$.

■ ASSOCIATED CONTENT

Ⓢ Supporting Information

Thermal data (Table S1), crystallographic data for complex **3** (Tables S2 and S3), spectroscopic characterization of the reaction intermediates, and a stability check in DMSO over time of complex **3** as the model compound (Figure S1). This material is available free of charge via the Internet at http://pubs.acs.org.

■ AUTHOR INFORMATION

Corresponding Author

*Phone: +39-(0)49-8275159, fax: +39-(0)2-700500560, e-mail: dolores.fregona@unipd.it.

■ ACKNOWLEDGMENTS

This work was supported by the European Union (Marie Curie European Re-Integration Grant 204828-PEPMIDAS to L.R.), Fondazione Cassa di Risparmio di Padova e Rovigo (www.fondazionecariparo.it), and Fondazione ABO (www.fondazioneabo.org). D.A. thanks Associazione Italiana per la Ricerca sul Cancro (AIRC) and Ministero della Salute (Ricerca Finalizzata FSN-IRCCS) for funding. The authors gratefully acknowledge Dr. Loris Calore for elemental analyses, Mrs. Cinzia Borghese and Dr. Naike Casagrande for assistance with

in vitro experiments, and colleagues of Centro Interdipartimentale di Ricerca "Ruolo degli Ioni Metallici nelle Scienze Biomediche" (BIOMÉTION) and of Consorzio Interuniversitario di Ricerca in Chimica dei Metalli nei Sistemi Biologici (CIRCMSB) for stimulating discussions.

■ ABBREVIATIONS USED

AA, amino acid; Aib, α-aminoisobutyric acid (α-methylalanine); BrdU, bromodeoxyuridine; DMSO, methyl sulfoxide; dpdtc, dipeptidedithiocarbamate; DSC, differential scanning calorimetry; dtc, dithiocarbamate; ELISA, enzyme-linked immunoadsorbent assay; FACS, fluorescence-activated cell sorting; FBS, fetal bovine serum; FITC, fluorescein isothiocyanate; HEPES, 4-(2-hydroxyethyl)-1-piperazineethanesulfonic acid; HMBC, heteronuclear multiple bond correlation; IBCF, isobutyl chloroformiate; IgG, immunoglobulin G; NMM, *N*-methylmorpholine; PEPT, peptide transporter; PI, propidium iodide; PS, phosphatidylserine; Sar, sarcosine (*N*-methylglycine); TEA, triethylamine; TG, thermogravimetry; THF, tetrahydrofuran; TMS, tetramethylsilane; Z-, benzyloxycarbonyl-; ZOSu, *N*-(benzyloxycarbonyloxy)succinimide

■ REFERENCES

(1) Kelland, L. The Resurgence of Platinum-Based Cancer Chemotherapy. *Nat. Rev. Cancer* **2007**, *7*, 573−584.
(2) Kostova, I. Platinum Complexes as Anticancer Agents. *Recent Pat. Anti-Cancer Drug Discovery* **2006**, *1*, 1−22.
(3) Sun, R. W. -Y; Ma, D. -L.; Wong, E. L. -M; Che, C. -M. Some Uses of Transition Metal Complexes as Anti-Cancer and Anti-HIV Agents. *Dalton Trans.* **2007**, 4884−4892.
(4) Bruijnincx, P. C. A.; Sadler, P. J. New Trends for Metal Complexes with Anticancer Activity. *Curr. Opin. Chem. Biol.* **2008**, *12*, 197−206.
(5) Nobili, S.; Mini, E.; Landini, I.; Gabbiani, C.; Casini, A.; Messori, L. Gold Compounds as Anticancer Agents: Chemistry, Cellular Pharmacology, and Preclinical Studies. *Med. Chem. Res.* **2010**, *30*, 550−580.
(6) Ott, I. On the Medicinal Chemistry of Gold Complexes as Anticancer Drugs. *Coord. Chem. Rev.* **2009**, *253*, 1670−1681.
(7) Tiekink, E. R. T. Anti-Cancer Potential of Gold Complexes. *Inflammopharmacology* **2008**, *16*, 138−142.
(8) Shimada, H.; Takahashi, K.; Funakoshi, T.; Kojima, S. Protective Effects of Dithiocarbamates Against Toxicity of cis-Diamminedichloroplatinum in Mice. *Biol. Pharm. Bull.* **1993**, *16*, 368−371.
(9) Ronconi, L.; Fregona, D. The Midas Touch in Cancer Chemotherapy: from Platinum- to Gold-Dithiocarbamato Complexes. *Dalton Trans.* **2009**, 10670−10680.
(10) Ronconi, L.; Aldinucci, D.; Dou, Q. P.; Fregona, D. Latest Insights into the Anticancer Activity of Gold(III)-Dithiocarbamato Complexes. *Anti-Cancer Agents Med. Chem.* **2010**, *10*, 283−292.
(11) Milacic, V.; Chen, D.; Ronconi, L.; Landis-Piwowar, K. R.; Fregona, D.; Dou, Q. P. A Novel Anticancer Gold(III) Dithiocarbamate Compound Inhibits the Activity of a Purified 20S Proteasome and 26S Proteasome in Human Breast Cancer Cell Cultures and Xenografts. *Cancer Res.* **2006**, *66*, 10478−10486.
(12) Zhang, X.; Frezza, M.; Milacic, V.; Ronconi, L.; Fan, Y.; Bi, C.; Fregona, D.; Dou, Q. P. Inhibition of Tumor Proteasome Activity by Gold Dithiocarbamato Complexes via both Redox-Dependent and -Independent Processes. *J. Cell. Biochem.* **2010**, *109*, 162−172.
(13) Cattaruzza, L.; Fregona, D.; Mongiat, M.; Ronconi, L.; Fassina, A.; Colombatti, A.; Aldinucci, D. Antitumor Activity of Gold(III)-Dithiocarbamato Derivatives on Prostate Cancer Cells and Xenografts. *Int. J. Cancer* **2011**, *128*, 206−215.
(14) Marzano, C.; Ronconi, L.; Chiara, F.; Giron, M. C.; Faustinelli, I.; Cristofori, P.; Trevisan, A.; Fregona, D. Gold(III)-Dithiocarbamato Anticancer Agents: Activity, Toxicology and Histopathological Studies in Rodents. *Int. J. Cancer* **2011**, *129*, 487−496.
(15) Rubio-Aliaga, I.; Daniel, H. Peptide Transporters and their Roles in Physiological Processes and Drug Disposition. *Xenobiotica* **2008**, *38*, 1022−1042.
(16) Brandsch, M.; Knütter, I.; Bosse-Doenecke, E. Pharmaceutical and Pharmacological Importance of Peptide Transporters. *J. Pharm. Pharmacol.* **2008**, *60*, 543−585.
(17) Brandsch, M. Transport of Drugs by Proton-Coupled Peptide Transporters: Pearls and Pitfalls. *Expert Opin. Drug Metab. Toxicol.* **2009**, *5*, 887−905.
(18) Valle, G.; Formaggio, F.; Crisma, M.; Bonora, G. M.; Toniolo, C.; Bavoso, A.; Benedetti, E.; Di Blasio, B.; Pavone, V.; Pedone, C. Linear Oligopeptides. Part 147. Chemical and Crystallographic Study of the Reaction between Benzyloxycarbonyl Chloride and α-Aminoisobutyric Acid. *J. Chem. Soc., Perkin Trans. 2* **1986**, 1371−1376.
(19) McGahren, W. J.; Goodman, M. Synthesis of Peptide Oxazolones and Related Compounds. *Tetrahedron* **1967**, *23*, 2017−2030.
(20) Vaughan, J. R. Jr.; Osato, R. L. Preparation of Peptides Using Mixed Carboxylic Acid Anhydrides. *J. Am. Chem. Soc.* **1951**, *73*, 5553−5555.
(21) Green, T. W.; Wuts, P. G. M. *Protective Groups in Organic Synthesis*; Wiley-Interscience: New York, 1999; pp 736−739.
(22) Ronconi, L.; Giovagnini, L.; Marzano, C.; Bettìo, F.; Graziani, R.; Pilloni, G.; Fregona, D. Gold Dithiocarbamate Derivatives as Potential Antineoplastic Agents: Design, Spectroscopic Properties, and in Vitro Antitumor Activity. *Inorg. Chem.* **2005**, *44*, 1867−1881.
(23) Shkaraputa, L. N.; Kononov, A. V.; Polackov, A. D. Preparation of Dithiocarbamates. *Ukr. Chem. J.* **1991**, *9*, 979−989.
(24) Vasiliev, A. N.; Polackov, A. D. Synthesis of Potassium (1,1-Dioxothiolan-3-yl)-dithiocarbamate. *Molecules* **2000**, *5*, 1014−1017.
(25) Colthup, N. B.; Daly, L. H.; Wiberley, S. E. *Introduction to Infrared and Raman Spectroscopy*; Academic Press: New York, 1990.
(26) Forghieri, F.; Preti, C.; Tassi, L.; Tosi, G. Preparation, Properties and Reactivity of Gold Complexes with some Heterocyclic Dithiocarbamates as Ligands. *Polyhedron* **1988**, *7*, 1231−1237.
(27) Beurskens, P. T.; Blaauw, H. J. A.; Cras, J. A.; Steggerda, J. J. Preparation, Structure, and Properties of Bis(*N*,*N*-dibutyldithiocarbamato)gold(III) Dihaloaurate(I). *Inorg. Chem.* **1968**, *7*, 805−810.
(28) Coates, G. E.; Parkin, C. Tertiary Phosphine Complexes of Trimethylgold: Infrared Spectra of Complexes of Gold and some Other Metals. *J. Chem. Soc.* **1963**, 421−429.
(29) Ronconi, L.; Maccato, C.; Barreca, D.; Saini, R.; Zancato, M.; Fregona, D. Gold(III) Dithiocarbamate Derivatives of N-methylglycine: an Experimental and Theoretical Investigation. *Polyhedron* **2005**, *24*, 521−531.
(30) Giovagnini, L.; Ronconi, L.; Aldinucci, D.; Lorenzon, D.; Sitran, S.; Fregona, D. Synthesis, Characterization and Comparative In Vitro Cytotoxicity Studies of Platinum(II), Palladium(II) and Gold(III) Methylsarcosinedithiocarbamate Complexes. *J. Med. Chem.* **2005**, *48*, 1588−1595.
(31) Wheate, N. J.; Walker, S.; Craig, G. E.; Oun, R. The Status of Platinum Anticancer Drugs in the Clinic and in Clinical Trials. *Dalton Trans.* **2010**, *39*, 8113−8127.
(32) Boulikas, T. Clinical Overview on Lipoplatin: a Successful Liposomal Formulation of Cisplatin. *Expert Opin. Invest. Drugs* **2009**, *18*, 1197−1218.
(33) Berners-Price, S. J; Filipovska, A. Gold Compounds as Therapeutic Agents for Human Diseases. *Metallomics* **2011**, *3*, 863−873.
(34) de Bono, J. S.; Ashworth, A. Translating Cancer Research into Targeted Therapeutics. *Nature* **2010**, *467*, 543−549.
(35) Strebhardt, K.; Ulrich, A. Paul Herlich's Magic Bullet Concept: 100 Years of Progress. *Nat. Rev. Cancer* **2008**, *8*, 473−480.
(36) Harper, B. W.; Krauser-Heuer, A. M.; Grant, M. P.; Manohar, M.; Garbutcheon-Singh, K. B.; Aldrich-Wright, J. R. Advances in Platinum Chemotherapeutics. *Chem.—Eur. J.* **2010**, *16*, 7064−7077.

(37) Noor, F.; Wüstholz, A.; Kinscherf, R.; Metzler-Nolte, N. A Cobaltocenium-Peptide Bioconjugate Shows Enhanced Cellular Uptake and Directed Nuclear Delivery. *Angew. Chem., Int. Ed.* **2005**, *44*, 2429−2432.
(38) Biegel, A.; Knütter, I.; Hartrodt, B.; Gebauer, S.; Theis, S.; Luckner, P.; Kottra, G.; Rastetter, M.; Zebisch, K.; Thondorf, I.; Daniel, H.; Neubert, K.; Brandsch, M. The Renal Type H^+/Peptide Symporter PEPT2: Structure-Affinity Relationships. *Amino Acids* **2006**, *31*, 137−156.
(39) Biegel, A.; Gebauer, S.; Hartrodt, B.; Brandsch, M.; Neubert, K.; Thondorf, I. Three-Dimensional Quantitative Structure−Activity Relationship Analyses of β-Lactam Antibiotics and Tripeptides as Substrates of the Mammalian H^+/Peptide Cotransporter PEPT1. *J. Med. Chem.* **2005**, *48*, 4410−4419.
(40) Nielsen, C. U.; Andersen, R.; Brodin, B.; Frokjaer, S.; Taub, M. E.; Steffansen, B. Dipeptide Model Prodrugs for the Intestinal Oligopeptide Transporter. Affinity for and Transport via hPepT1 in the Human Intestinal Caco-2 Cell Line. *J. Controlled Release* **2001**, *76*, 129−138.
(41) Sugawara, M.; Huang, W.; Fei, Y. J.; Leibach, F. H.; Ganapathy, V.; Ganapathy, M. E. Transport of Valganciclovir, a Ganciclovir Prodrug, via Peptide Transporters PEPT1 and PEPT2. *J. Pharm. Sci.* **2000**, *89*, 781−789.
(42) Rubio-Aliaga, I.; Daniel, H. Mammalian Peptide Transporters as Targets for Drug Delivery. *Trends Pharmacol. Sci.* **2002**, *23*, 434−440.
(43) Mitsuoka, K.; Miyoshi, S.; Kato, Y.; Murakami, Y.; Utsumi, R.; Kubo, Y.; Noda, A.; Nakamura, Y.; Nishimura, S.; Tsuji, A. Cancer Detection Using a PET Tracer, ^{11}C-Glycylsarcosine, Targeted to H^+/Peptide Transporter. *J. Nucl. Med.* **2008**, *49*, 615−622.
(44) Landowski, C. P.; Vig, B. S.; Song, X.; Amidon, G. L. Targeted Delivery to PEPT1-Overexpressing Cells: Acidic, Basic, and Secondary Floxuridine Amino Acid Ester Prodrugs. *Mol. Cancer Ther.* **2005**, *4*, 659−667.
(45) Aldinucci, D.; Ronconi, L.; Fregona, D. Groundbreaking Gold(III) Anticancer Agents. *Drug Discovery Today* **2009**, *14*, 1075−1076.
(46) Geissler, S.; Zwarg, M.; Knütter, I.; Markwardt, F.; Brandsch, M. The Bioactive Dipeptide Anserine is Transported by Human Proton-Coupled Peptide Transporters. *FEBS J.* **2010**, *277*, 790−795.
(47) Picquart, M.; Abedinzadeh, Z.; Grajcar, L.; Baron, M. H. Spectroscopic Study of N-Acetylcysteine and N-Acetylcystine/Hydrogen Peroxide Complexation. *Chem. Phys.* **1998**, *228*, 279−291.
(48) Fillaux, F.; De Lozé, C. Spectroscopic Study of Monosubstituted Amides. II. Rotation Isomers in Amides Substituted by Aliphatic Side-Chain Models. *Biopolymers* **1972**, *11*, 2063−2077.
(49) Fillaux, F.; De Lozé, C. Structure of Matrix Isolated N-Methylacetamide. *Chem. Phys. Lett.* **1976**, *39*, 547−551.
(50) Lin-Vien, D.; Colthup, N. B.; Fateley, W. G.; Grasselli, J. G. *Infrared and Raman Characteristic Frequencies of Organic Molecules*; Academic Press: London, 1991; pp 144−145.
(51) Bonati, F.; Ugo, R. Organotin(IV) N,N-Disubstituted Dithiocarbamates. *J. Organomet. Chem.* **1967**, *10*, 257−268.
(52) van Gaal, H. L. M.; Diesveld, J. W.; Pijpers, F. W.; van der Linden, J. G. M. ^{13}C NMR Spectra of Dithiocarbamates. Chemical Shifts, Carbon-Nitrogen Stretching Vibration. *Inorg. Chem.* **1979**, *18*, 3251−3260.
(53) Cras, J. A.; Willemse, J. Dithiocarbamates and Related Ligands. In *Comprehensive Coordination Chemistry. The Synthesis, Reactions, Properties and Applications of Coordination Compounds*; Wilkinson, G.; Gillard, R. D.; McCleverty, J. A., Eds.; Pergamon Press: Oxford, 1987; pp 579−593.
(54) Dempsey, C. E. Hydrogen Exchange in Peptides and Proteins Using NMR Spectroscopy. *Prog. Nucl. Magn. Reson. Spectrosc.* **2001**, *39*, 135−170.
(55) Bakir, M.; Conry, R. R.; Green, O. X-Ray Crystallographic and Molecular Sensing Properties of $[ZnCl_2(\kappa^2\text{-}N,N'\text{-dpknph})]$ (dpknph = di-2-pyridylketone-*p*-nitrophenyl hydrazone). *J. Mol. Struct.* **2008**, *889*, 35−44.
(56) Brown, K. L.; Hancock, R. E. W. Cationic Host Defense (Antimicrobial) Peptides. *Curr. Opin. Immunol.* **2006**, *18*, 24−30.
(57) Johnstone, S. A.; Gelmon, K.; Mayer, L. D.; Hancock, R. E.; Bally, M. B. In Vitro Characterization of the Anticancer Activity of Membrane-Active Cationic Peptides. I. Peptide-Mediated Cytotoxicity and Peptide-Enhanced Cytotoxic Activity of Doxorubicin against Wild-Type and p-Glycoprotein Overexpressing Tumor Cell Lines. *Anti-Cancer Drug Des.* **2000**, *15*, 151−160.
(58) Toniolo, C.; Brückner, H. *Peptaibiotics*; Wiley-VCD/VHCA: Weinheim/Zürich, 2009.
(59) Fregona, D.; Ronconi, L.; Marzano, C. Dithiocarbamate Complexes of Gold(III) and their Use as Antitumor Agents. Ital. Pat. IT1347835B1, 2008.
(60) Fregona, D.; Ronconi, L.; Formaggio, F.; Dou, Q. P.; Aldinucci, D. Gold(III) Complexes with Oligopeptides Functionalized with Sulfur Donors and Use thereof as Antitumor Agents. PCT Int. Appl. WO2010105691A1, 2010.
(61) Fulmer, G. R.; Miller, A. J. M.; Sherden, N. H.; Gottlieb, H. E.; Nudelman, A.; Stoltz, B. M.; Bercaw, J. E.; Goldberg, K. I. NMR Chemical Shifts of Trace Impurities: Common Laboratory Solvents, Organics, and Gases in Deuterated Solvents Relevant to the Organometallic Chemist. *Organometallics* **2010**, *29*, 2176−2179.
(62) *SMART (Control) and SAINT (Integration) Software for CCD Systems*; Bruker AXS Inc., Madison, WI, 1994.
(63) *Area-Detector Absorption Correction*; Siemens Industrial Automation Inc.:, Madison, WI, 1996.
(64) Burla, M. C.; Caliandro, R.; Camalli, M.; Carrozzini, B.; Cascarano, G. L.; De Caro, L.; Giacovazzo, C.; Polidori, G.; Spagna, R. SIR2004: an Improved Tool for Crystal Structure Determination and Refinement. *J. Appl. Crystallogr.* **2005**, *38*, 381−388.
(65) Sheldrick, G. M. *SHELX-97. Programs for Crystal Structure Analysis (Release 97-2)*; University of Göttingen, Göttingen, Germany, 1997.
(66) Farrugia, L. J. WinGX Suite for Small-Molecule Single-Crystal Crystallography. *J. Appl. Crystallogr.* **1999**, *32*, 837−838.
(67) Farrugia, L. J. ORTEP-3 for Windows - A Version of ORTEP-III with a Graphical User Interface (GUI). *J. Appl. Crystallogr.* **1997**, *30*, 565−568.
(68) Andrews, P. A.; Murphy, M. P.; Howell, S. B. Differential Potentiation of Alkylating and Platinating Agent Cytotoxicity in Human Ovarian Carcinoma Cells by Glutathione Depletion. *Cancer Res.* **1985**, *45*, 6250−6253.
(69) Santa Cruz Biotechnology, http://www.scbt.com/protocols.html.
(70) Profit, S.; Unteregger, G. Quantitative Measurement of Cell Proliferation Using the BrdU ELISA: a Comparison between Colorimetric and Chemiluminescent Detection. *Biochemica* **2001**, *4*, 33−35.
(71) Stroben, W. Trypan Blue Exclusion Test of Cell Viability. In *Current Protocols in Immunology*; Coligan, J. E., Bierer, B., Margulies, D. H., Shevach, E. M., Strober, W., Coico, R., Eds.; John Wiley & Sons: New York, 2001; appendix 3B.
(72) Aldinucci, D.; Lorenzon, D.; Stefani, L.; Giovagnini, L.; Colombatti, A.; Fregona, D. Antiproliferative and Apoptotic Effects of Two New Gold(III) Methylsarcosinedithiocarbamate Derivatives on Human Acute Myeloid Leukemia Cells In Vitro. *Anti-Cancer Drugs* **2007**, *18*, 323−332.